NICOTINIC ACETYLCHOLINE RECEPTORS IN BREAST CANCER

THE USE OF NICOTINIC ACETYLCHOLINE RECEPTOR ANTAGONISTS TO TARGET BREAST TUMOR-INITIATING CELLS

By MELISSA KATHLEEN BEILSCHMIDT, B.Sc. (Hons.)

A Thesis Submitted to the School of Graduate Studies in Partial

Fulfillment of the Requirements for the Degree Master of Science

McMaster University

MASTER OF SCIENCE (2014) McMaster University (Medical Sciences)
Hamilton, Ontario

Title: The Use of Nicotinic Acetylcholine Receptor Antagonists to Target Breast Tumor-Initiating Cells

Author: Melissa Kathleen Beilschmidt, B.Sc. (Hons.)

Supervisor: Dr. John A. Hassell

Number of pages: xii, 93

ABSTRACT

The high rate of relapse often seen in breast cancer patients has been suggested to be the result of a small subset of chemotherapy-resistant cancer stem cells (CSCs), believed to be responsible for initiating tumor formation. These CSCs possess the capability to self-renew and give rise to a hierarchy of cells which makes up the bulk of a tumor. Neurotransmitters have been suggested to influence CSC self-renewal and proliferation capabilities, and antagonists of neurotransmission pathways have been implicated as possible treatment methods for chemo-resistant tumors. Using nicotinic acetylcholine receptor (nAChR) antagonists in sphere-forming assays, we have identified a very promising candidate compound: MG624. We found this compound to have a high selectivity for sphere-forming cells over non-sphere-forming cells *in vitro*, in a dose-dependent relationship, across a panel of cell lines as well as in patient-derived xenograft cells. This was validated in two *ex vivo* assays, where tumor formation was significantly delayed in mice injected with MG624-treated HCC1954 cells at both the IC_{50} and IC_{90} of the compound, indicating that MG624 does indeed target functional BTICs. MG624 was also found to synergize with both taxotere and doxorubicin chemotherapies *in vitro*, and shrink tumors in NOD/SCID mice when combined with taxotere *in vivo*. MG624 in combination with taxotere was found to induce apoptosis, and prevent cells from entering into the M-phase of the cell cycle. Interestingly, MG624 was found to eliminate intratumoral fibroblasts in combination with taxotere, despite taxotere being found to recruit fibroblasts to the tumor site when used on its own. Most importantly, the combination of MG624 and taxotere was found to significantly delay tumor

progression/relapse in mice, indicating that MG624 may be an excellent candidate compound to one day be combined with chemotherapy to provide durable remission to breast cancer patients.

ACKNOWLEGEMENTS

The first person I would like to acknowledge and thank is my M.Sc. supervisor Dr. John Hassell for his guidance and mentorship throughout the course of my research. He granted me the independence required to fully immerse myself in my research project, and let me make mistakes along the way (with minor razzing, of course), allowing me to fully understand the importance of proper experimental design and planning. John always keeps me laughing, which made for an awesome 2 years in his lab.

I would also like to thank my committee members Drs. Anita Bane and Sheila Singh for their helpful suggestions and assistance in interpreting my data, and identifying areas for future research. I would also like to acknowledge and thank all past and present members of the Hassell lab, particularly Adele for all of her help with cell culture and immunofluorescence, Craig for his assistance with patient-derived xenografts, and notably Dr. Robin Hallett for his endless guidance and support. He encouraged critical analysis of my data, building on my understanding that biology is never black and white, and brought me back down to reality when I let myself run wild with an untested theory. He also greatly assisted me in terms of mouse work and experimental design, and motivated me when I became frustrated or ambivalent. For that, I will be forever grateful.

Finally, I would like to thank my husband Eric for his encouragement and understanding, especially when I became emotional or stressed. He has kept me level headed and focused on the bigger picture, and I truly want to thank him for being so supportive.

TABLE OF CONTENTS

LIST OF TABLES

LIST OF FIGURES

LIST OF ABBREVIATIONS

αBgtx: Alpha-bungarotoxin

ACh: Acetylcholine

ALDH: Alcohol dehydrogenase

αSMA: Alpha smooth muscle actin

ANOVA: Analysis of variance

ATCC: American Type Culture Collection

BTIC: Breast tumor-initiating cell

CAF: Cancer-associated fibroblasts

CCAC: Canadian Council on Animal Care

CK8: Cytokeratin-8

CSC: Cancer stem cell

DMEM: Dulbecco's modified eagle medium

DNA: Deoxyribonucleic acid

ECM: Extracellular matrix

EGF: Epidermal growth factor

EGFR: Epidermal growth factor receptor

EMT: Epithelial mesenchymal transition

EpCAM: Epithelial cell adhesion molecule

ER: Estrogen receptor

ESA: Epithelial-specific antigen

EtOH: Ethanol

FACS: Fluorescent activated cell sorting

FAP: Fibroblast activation protein

FBS: Fetal bovine serum

FGF: Fibroblast growth factor

G1/2/3: Generation 1/2/3

H&E: Hematoxylin and eosin

HEPA: High-efficiency particulate air

HER2: Human epidermal growth factor receptor 2

HuMt: Human mitochondria

IC_{50}: Inhibitor concentration 50

IP: Intraperitoneal

mAChR: Muscarinic acetylcholine receptor

MTD: Maximum tolerated dose

nAChR: Nicotinic acetylcholine receptor

NGF: Nerve growth factor

NGS: Normal goat serum

NOD/SCID: Non-obese diabetic/severe combined immunodeficiency

NSG: Non-obese diabetic/severe combined immunodeficiency gamma

PAH: Polycyclic aromatic hydrocarbons

PBS: Phosphate buffered saline

PBST: Phosphate buffered saline with 0.03% Tween-20

PDAC: Pancreatic ductal adenocarcinoma

PDX: Patient-derived xenograft

Pen/Strep: Penicillin/streptomycin

PR: Progesterone receptor

RNA: Ribonucleic acid

RPMI: Roswell Park Memorial Institute medium

SCLC: Small cell lung cancer

SCM: Stem cell media

SD: Standard deviation

SEM: Standard error mean

%SphINH: Percent sphere inhibition

TIC: Tumor-initiating cell

TSN: Tobacco-Specific nitrosamine

TUNEL: Terminal deoxynucleotidyl transferase dUTP nick end labeling

CHAPTER 1: INTRODUCTION

Breast cancer

Breast cancer is the leading cause of cancer-related death in women worldwide (Ferlay *et al.*, 2013), and it is estimated that one in eight women will get breast cancer in her lifetime (Siegel *et al.*, 2012). Over the past 15 years, there has been a great deal of advancement in the understanding of breast cancer, including its pathogenesis, biological diversity and different etiologic pathways involved in breast cancer development (Allison, 2012). One important breakthrough in the field of breast cancer research has been the discovery that breast cancer is not a single disease, but rather a collection of diseases of the breast with unique genetic diversities, growth rates, clinical presentations and patient outcomes (Polyak, 2007; Vargo-Gogola & Rosen, 2007). Multiple molecular subtypes of breast cancer have been described from gene expression profiling of invasive breast cancers (Perou *et al.*, 2000; Hu *et al.*, 2006; Neve *et al.*, 2006). The five most commonly identified breast cancer subtypes include luminal A tumors, which are estrogen receptor (ER)-positive, and are often more differentiated, and non-invasive (low grade); luminal B tumors, which are also ER-positive but often less differentiated and more invasive (high grade); basal-like breast tumors, often referred to as triple negative tumors, meaning ER-negative, progesterone receptor (PR)-negative; and human epidermal growth factor receptor 2 (HER2)-negative; HER2+ breast tumors, which overexpress the *HER2* gene; and a normal breast-like subgroup, which has been found to express adipose tissue genes, and may be an artifact of normal tissue contamination.

Advances in diagnostic techniques and an increase in breast cancer screening has led to earlier diagnosis in patients (Evans *et al.*, 2013). Despite those advancements, breast cancer treatment options are relatively restricted to surgery (either lumpectomy or mastectomy) in combination with radiotherapy (Veronesi *et al.*, 2002), and either neo-adjuvant (before surgery) or adjuvant (after surgery) chemotherapy, or endocrine therapy. By comparison to the advancements made in the field of breast cancer research with regards to diagnostics and screening, our understanding of the factors involved in tumor progression and the development of methods to interfere with tumor progression are quite limited (Polyak, 2007).

Most chemotherapeutics function by targeting rapidly proliferating cells, often via DNA damage (Ma *et al.*, 2013). Unfortunately, chemotherapy also damages normal tissues causing undesirable side effects, and there are many long-term negative health effects of chemotherapy regimens that are exponentially dose-dependent (Azim *et al.*, 2011). These long-term health consequences include cardiac toxicity (Swain *et al.*, 2003), secondary non-breast cancers (Schaapveld *et al.*, 2008), cognitive impairment (Player *et al.*, 2014), reduced fertility (Partridge *et al.*, 2008), and an overall decreased quality of life. Therefore, it is ideal to give the lowest dose of chemotherapy possible that will still lead to long-term disease-free survival.

Unfortunately, while most breast cancer patients initially respond to conventional chemotherapeutics, many have been found to relapse over time, with relapse rates being reported as being as high as 40%, depending on the extent of breast tissue removed, the combination of chemotherapy used, and the size of the primary tumor (Rosen *et al.*, 1989;

Mansi *et al.*, 2010). Many hypotheses have been proposed to explain this high rate of recurrence and ultimate treatment failure. One hypothesis is that a small subpopulation of cells within a tumor, deemed breast tumour-initiating cells (BTICs) or cancer stem cells (CSCs), may be responsible for reinitiating tumor growth after treatment.

Cancer stem cells

Stem cells are generally defined by two important properties: the ability to self-renew, and the ability to divide into more differentiated daughter cells, making up the mature cells of a specific tissue (Dontu *et al.*, 2003; Magee *et al.*, 2012). The self-renewal element of stem cells is their ability to go through multiple mitotic cell divisions, without further differentiating. These cells give rise to each cell type found in a given organ or gland, and are therefore of considerable interest for tissue regeneration (Dontu *et al.*, 2003). In tumours, cells with stem cell-like properties have been identified, and are therefore referred to as CSCs, or tumor-initiating cells (TICs).

Tumours are made up of a heterogeneous array of cells, which may be attributed to a hierarchal organisation within the tumour, beginning with a CSC. CSCs are believed to be responsible for tumor formation, whereas their differentiated progeny have been found, in many cancer types, to lose their proliferative potential despite maintaining the same genetic makeup present in the undifferentiated progenitor cells which gave rise to them (Magee *et al.*, 2012). Differentiated cells are also capable of becoming tumorigenic, through mutations that activate self-renewal mechanisms (Visvader & Lindeman, 2012).

Therefore, the cancer stem cell model does not identify a cell of origin, nor does it claim that cancer stem cells arise from normal stem cells.

It is difficult to distinguish a 'differentiated' cancer cell from a CSC in a tumor based on phenotypic traits alone (Dontu *et al.*, 2003). A number of markers have been found to be highly expressed on the surface of CSCs compared to their more differentiated progeny, including CD133, $CD44^{+}/CD24^{-}$, ESA^{+} (epithelial-specific antigen) or EpCAM (epithelial cell adhesion molecule), and ALDH (Alcohol dehydrogenase) (Fillmore & Kuperwasser, 2008; May *et al.*, 2011; Visvader & Lindeman, 2012), however the classic model used to demonstrate the presence of CSCs is to serially transplant cancer cell lines into immunocompromised mice (Baccelli & Trumpp, 2012)., i.e. limiting dilution cell transplantations (Kondratyev *et al.*, 2012). It has been found that the minimum number of cells required to initiate a tumour, while variable across different cancer subtypes, is quite high, indicating that TICs are relatively rare (Quintana *et al.*, 2008).

Accumulating evidence has demonstrated that TICs are resistant to conventional cancer therapeutics (Sachlos *et al.*, 2012), including both chemotherapy (Li *et al.*, 2008) and radiation (Woodward *et al.*, 2007). One reason for this resistance is due to CSCs expressing high levels of ATP-binding cassette (ABC) transporters, which actively efflux drugs from cells, protecting them from the cytotoxic effects of chemotherapeutics (Dean *et al.*, 2005). However, inhibition of these transporters was quite unsuccessful in clinical trials against lung (Millward *et al.*, 1993), breast (Wishart *et al.*, 1994) and colon cancers

(Lhommé *et al.*, 2008) indicating that other factors may be involved in TIC drug resistance.

The interaction of CSCs with their microenvironment has been found to be crucial for seeding metastases, and metastatic growth (Sleeman & Cremers, 2007), and recently it has been shown to play a role in TIC chemoresistance. For example, co-culturing chemotherapy-treated cancer-associated fibroblasts (CAFs) and colorectal CSCs was found to increase the viability, self-renewal and chemoresistance of CSCs through IL-17A secretion (Lotti *et al.*, 2013). CAFs synthesize fibroblast activation protein (FAP), which is involved in extracellular matrix (ECM) remodelling, and fibroblasts regulate tension applied to the ECM, thereby modulating interstitial fluid pressure, decreasing tumor chemotherapeutic drug uptake. Interestingly, CD8+ T-cell-mediated killing of CAFs has been found to suppress tumor growth and metastasis and decrease collagen type I expression, leading to a 70% greater chemotherapeutic drug uptake in colon carcinomas (Loeffler *et al.*, 2006). The chemoresistant nature of TICs would explain why some tumours may initially regress during cancer therapies and how recurrence could be attributed to the drug resistant "side population" of TICs (Goodell *et al.*, 1996).

In breast cancer, Brca1-deficient mouse mammary tumours were used to demonstrate a drug-resistant population of cells expressing $CD44^{+}/CD24^{-}$, which were also found to over-express ABC transporters, and form spheres in culture (Wright *et al.*, 2008). Another study found that residual breast tumour populations remaining after chemotherapy were enriched for cells containing the $CD44^{+}/CD24^{-}$ phenotype, and these cells also displayed mesenchymal features (Creighton *et al.*, 2009). These studies are

complemented by the fact that chemotherapy patients whose tumour mass following neo-adjuvant chemotherapy consists of mainly differentiated cells have a much better prognosis than patients whose remaining tumour cells consist primarily of undifferentiated progenitor cells (Magee *et al.*, 2012). Therefore, targeting breast CSCs may be necessary in order to provide a durable cure for breast cancer patients.

Propagating TICs in culture

In an adherent cell culture, the percentage of stem cells is quite rare. However Weiss *et al* (1996) proposed that non-adherent sphere cultures could be used to purify undifferentiated, progenitor cells, using serum-free media supplemented with growth factors and insulin. This technique was used to propagate multipotent neuronal stem cells, giving rise to suspensions of neurospheres consisting of 4%-20% stem cells, with the remaining cells existing in a further differentiated, progenitor-like state (Weiss *et al.*, 1996). In 2003, Dontu *et al* demonstrated the use of this method to grow nonadherent mammospheres; human mammary epithelial cells grown in suspension in serum-free media containing EGF, bFGF, hydrocortisone, insulin, B27, and heparin to produce spheres similar to the neurospheres propagated by Weiss *et al* (1996) (Dontu *et al.*, 2003). These three dimensional (3D) sphere cultures are now used to enrich for and propagate many different types of CSCs, including lung (Levina *et al.*, 2010), breast (Fillmore & Kuperwasser, 2008), and kidney CSCs (Su *et al.*, 2013).

CSCs grown in non-adherent sphere cultures that are believed to initiate sphere formation and give rise to the further differentiated cells within a sphere are called sphere-forming cells whereas CSCs that initiate tumors in mice are referred to as TICs.

Sphere-forming assays are often used to test compounds believed to target CSCs. The sphere-forming assay is based on the assumption that each sphere that forms directly corresponds to the number of viable sphere-forming cells seeded in each well, thus is a sensitive assay for directly assessing a compound's effect on sphere-forming cells, instead of on breast cancer cells in general. Nomenclature is important for CSC proponents, as sphere-forming cells are believed to be analogous to TICs, however technically speaking they are not one in the same. In fact, sphere-forming cell numbers often do not provide an accurate read out of CSCs *in vivo* (Pastrana *et al.*, 2011). Therefore, as previously mentioned, the gold standard used to measure the efficacy of CSC-targeted therapies is serial dilution cell transplants into immunocompromised mice. TICs are functional CSCs, and while spheres are enriched for TICs, they never contain a pure population of TICs. Thus, while sphere-forming assays are an inexpensive, robust method to test compounds that target TICs, they are not definitive proof that a compound targets TICs. Therefore compounds are often screened in sphere-forming assays and then validated *in vivo*.

Preliminary data and scientific rationale

Due to the chemotherapy-resistant population of BTICs believed to be responsible for the high rate of relapse seen in breast cancer patients, a durable cure for breast cancer will involve targeting BTICs as well as their decedents (either alone or in combination with conventional chemotherapy). Therefore, in attempt to identify compounds that might target BTICs, my lab identified gene signatures focusing on specific TIC-like properties. In particular, one data set involved comparative gene expression profiling of 14 patient breast tumor biopsies flow-sorted by $CD44^{+}/CD24^{-/low}$ vs. others (publically available

data) (Creighton *et al.*, 2009). The other signature was developed in our lab involving a panel of 10 breast cancer cell lines screened for their response to Adriamycin (doxorubicin) chemotherapy. The gene expression profiles of the four most chemosensitive and the four most chemoresistant cell lines were then downloaded (E-TABM-157) (Neve *et al.*, 2006) and compared, with the resultant differentially expressed genes being used as a signature for chemotherapy resistance (Hallett, 2012). Therefore one signature represented a phenotypical identification of BTICs ($CD44^{+/}CD24^{-/low}$ marker expression), whereas the other represented a functional characteristic of TICs (chemotherapy resistance). These signatures were then independently used to complete connectivity mapping, a technique that connects transcript-based signatures with the activity of small molecules (Lamb *et al.*, 2006), which has been successfully used by other investigators to identify novel anticancer compounds (Hassane *et al.*, 2008). Using this database, a "query signature" representing a particular biological state of interest (i.e. chemosensitivity or $CD44^{+}/CD24^{-/low}$ expression) can be used to search for small molecules that may perturb either the $CD44^{+}/CD24^{-/low}$ signature, or the chemotherapy response signature. Interestingly, both of our independent TIC signatures identified adiphenine, a local anesthetic and acetylcholine receptor (AChR) antagonist that binds to both muscarinic (Guy & Hamor, 1973) and nicotinic (Spitzmaul *et al.*, 2009) receptors, as an anti-TIC agent. A summary of the identification of adiphenine as a potential anti-TIC compound, and the process most often used in our lab to test compounds for their anti-TIC capabilities can be found in Figure 1.

In order to determine which AChR adiphenine binds to inhibit TICs, chemosensitization assays were performed. Chemoresistance is a functional property of TICs. Therefore the hypothesis of this experiment was that a compound that targets TICs would sensitize breast cancer cells to chemotherapy. Thus adiphenine as well as a variety of other mAChR and nAChR antagonists were used in chemosensitization assays in order to determine which AChR adiphenine specifically antagonizes to produce its chemosensitizing effects. To this end, 9 nicotinic acetylcholine receptor antagonists, and 6 muscarinic receptor antagonists were chosen to be used in chemosensitivity assays. Eight out of 9 nicotinic acetylcholine receptor (nAChR) antagonists were found to display chemosensitizing abilities, compared to 1 out of the 6 muscarinic acetylcholine receptor (mAChR) antagonists (Hallett, 2012). Therefore, nAChRs were hypothesized to be involved in breast CSC survival.

Nicotinic acetylcholine receptors and cancer

Nicotinic acetylcholine receptors

The discovery that interneuronal communication involves chemical messengers and not electrical transmission was one of the greatest scientific breakthroughs of the twentieth century (López-Muñoz & Alamo, 2009). Acetylcholine (ACh), one of the most important neurotransmitters in the nervous system (Lin *et al.*, 2012), was the first neurotransmitter ever discovered (Dale & Dudley, 1929; Brown, 2006; Sourkes, 2009; Taly *et al.*, 2009). There are two types of membrane ACh receptors: the G protein-coupled muscarinic ACh receptor (mAChR), and the nicotinic acetylcholine receptor (nAChR). The nAChR was the first neurotransmitter receptor and ion channel ever

isolated (López-Muñoz & Alamo, 2009; Corringer *et al.*, 2012). nAChRs are composed of hetero- or homo-pentamers of five subunits that enclose a central ion channel (Millar, 2003; Lin *et al.*, 2012). Each subunit contains 3 hydrophobic transmembrane domains (M1-M3), a large intracellular loop, followed by a fourth hydrophobic transmembrane domain (M4). Before the first domain, there is a disulfide-bonded cys loop, consistent with the cys-loop family of ion channels (Amici *et al.*, 2012; Lin *et al.*, 2012). There are two types of nAChRs: muscle and neuronal, each with their own unique combination(s) of subunits that form these pentameric receptors. Muscle nAChRs are made up of α1, β1, γ, δ and ε. Neuronal nAChRs are made up of a combination of α2-α10, and β2-β4. There are two distinct classes of neuronal nAChRs; one that binds αBgtx with nM affinity, but all other agonists with μM affinity, also known as αBgtx-nAChRs, and the other one that binds acetylcholine and nAChR agonists with nM affinity, but not α-Bungarotoxin (αBgtx), henceforth referred to as non-αBgtx nAChRs, The αBgtx class of nAChRs can assemble as 5 homomeric subunits (made up of α7-α9 homo-pentamers), or they can assemble to form heteromeric receptors, made up of either α7, α8, or α9, α10 subunits (Gotti & Clementi, 2004). The non-αBgtx nAChRs, on the other hand, only form heteropentamers, made up of two subunits, an α and a non-α subunit, containing α2-α6 and β2-β4 subunits (Bertrand *et al.*, 1990; Gotti & Clementi, 2004; D'hoedt & Bertrand, 2009). The complexity of the different combinations of nAChR subunits possible is not fully understood. For instance, neither the α5 nor the β3 subunits can form functional channels unless they are co-expressed with both an α and β subunit (Gotti & Clementi, 2004), and are thus referred to as auxiliary subunits. They do not participate in the ligand

binding site, but may play a role in ion permeability (Gotti & Clementi, 2004). These pentameric structures have subunits organised around a central ion channel. The ACh binding site is located at the interface between two adjacent subunits. The principal component of the binding site is located on the α-subunit. The complementary binding site is located on the adjacent subunit.

Nicotine is well-known for being an AChR agonist, binding to the same binding site as ACh. When ACh or nicotine bind to nAChRs, this causes a conformational change in the receptor, opening the ligand-gated ion channel on the intracellular side (Egleton *et al.*, 2008; D'hoedt & Bertrand, 2009; Schuller, 2009; Lin *et al.*, 2012). This allows for the influx of a variety of cations, including Na^+, K^+, and Ca^{2+} , leading to membrane depolarization. This causes the opening of voltage-gated Ca^{2+} channels, leading to an even greater influx of Ca^{2+} (Schuller, 2009). The cellular influx of Ca^{2+} leads to a variety of cellular responses, including an assortment of signaling cascades involved in cell proliferation, apoptosis and migration. The ion influx also triggers the release of neurotransmitters (including serotonin and dopamine), as well as growth factors, growth factor receptors and angiogenic factors (Egleton *et al.*, 2008; Prevarskaya *et al.*, 2010).

While nAChRs were characterized in neuronal cells, they have also been found to be present in non-neuronal cells as well, including muscle and lymphoid tissue, skin, lung cells, vascular tissue, macrophages and astrocytes (Gotti & Clementi, 2004) and more importantly, in cancer cells (Egleton *et al.*, 2008).

Neurotransmission and cancer

In the past 30 years, tumor initiation research has been mainly focused on chemical carcinogens (Wogan *et al.*, 2004; Battershill, 2005; Weinberg, 2014), which has been the basis of cancer prevention and intervention strategies (Schuller, 2008). However, carcinogens alone do not explain the vast complexity of cancer development, and it has become evident that cancer initiation and progression occurs through a wide variety of mechanisms, with DNA mutations and deletions being only one of the many factors involved (Hanahan & Weinberg, 2011). For example, the well-known association between smoking and virtually all forms of cancer, particularly lung cancer, has been thought to be directly related to the carcinogenic compounds in tobacco. However, nicotine has now been shown to play a vital role in cancer development as well.

Tobacco contains over 4000 chemicals, of which over 70 have been identified as carcinogenic (Hecht, 2012). These include tobacco-specific nitrosamines (TSNs), mainly n-nitroso-nornicotine (NNN) and 4-(methylnitrosamino)-1-(3-pyridyl)-1-butanone (NNK), as well as polycyclic aromatic hydrocarbons (PAHs). PAHs are mainly found in tar, contained in the particulate matter fraction of smoke, which has been greatly reduced through the introduction of cigarette filters which trap the tar. TSNs, on the other hand, are formed from nicotine in mammals (Schuller, 2008). In 1989, it was discovered that both NNK and nicotine stimulated human small cell lung cancer cells (SCLCs) by binding to nAChRs (Schuller, 1989), indicating that these receptors may be key regulators of many human cancers, and that the carcinogens alone may not be the sole reason cigarettes have been found to be linked to so many forms of cancer. nAChR signalling is

not the only neurotransmission pathway activated in cancer development. Other neurotransmission pathways have also been implicated in cancer initiation and progression, including β-adrenergic signaling in pancreatic ductal adenocarcinoma (PDAC) cells (Schuller, 2008), and serotonin signaling in prostate cancer cells (Siddiqui *et al.*, 2006).

Neurotransmitters are secreted by neurons, where they travel across synapses from one neuron to another. While there is a limited body of evidence demonstrating neurotransmitters are secreted by some tumor cell types for autocrine or paracrine signalling, mainly lung cancer cells synthesizing and secreting ACh (Song *et al.*, 2003; Song & Spindel, 2008), key ACh breakdown enzymes, such as acetylcholinesterase (AChE) have been detected in a variety of cancer cells, including breast cancer (Ruiz-Espejo *et al.*, 2002). Additionally, tumors have been found to secrete neurogenic factors (Geldof *et al.*, 1998; Ricci *et al.*, 2001), and axon guiding molecules, which have been found to play a role in tumorigenesis (Chédotal *et al.*, 2005). Nerve fibers have been found in bladder tumors (Seifert *et al.*, 2002), intraocular tumors (Seifert & Spitznas, 2001), prostate cancer (Ventura *et al.*, 2002), breast cancer (Tsang & Chan, 1992; Mitchell *et al.*, 1994), and in tissues of choroidal melanoma (Seifert & Spitznas, 2002). Interestingly, the presence of nerve fibers in colorectal cancer has been associated with poorer outcome (Grabowski *et al.*, 2001). Dollé *et al* (2003) demonstrated that breast cancer cells produce and secrete biologically active nerve growth factor (NGF), whereas normal breast cells do not (Dollé *et al.*, 2003), demonstrating the intrinsic ability of tumors to induce their own innervation (neoneurogenesis), using a similar mechanism to

how tumors induce angiogenesis, and lymphangiogenesis (Entschladen *et al.*, 2008; Mancino *et al.*, 2011).

Many neurotransmission pathway antagonists have been found to effect neuronal precursor cells, inhibiting or reducing neurosphere formation. Thus it has been hypothesized that many of these neurotransmitters (i.e. dopamine, serotonin, acetylcholine, norepinephrine, etc.) may influence the fate of these precursor cells by functioning in an elaborate network of signalling pathways (Diamandis *et al.*, 2007). Many gene expression profiles of brain tumours share many similarities to neuronal precursor cells, and as would be expected, compounds that were found to inhibit normal neuronal stem cell populations have also been found to inhibit brain CSC self-renewal and proliferation capabilities (Diamandis *et al.*, 2007). Therefore, it is understandable why nAChRs have been implicated in many cancers, including breast cancer (Schuller, 2009).

Nicotine and tumorigenesis

More than 5 million people die each year from the consequences of cigarette smoking (Changeux, 2010). Smoking is well known to be the leading risk factor for lung cancer, however it is also implicated in many other cancer subtypes, including breast cancer. According to the CPS-II Nutrition Cohort, a prospective study involving 73 000 postmenopausal women, current or former smokers have a higher incidence of invasive breast cancer compared to never smokers, and this risk was even higher in women who began smoking at an early age (Sagiv *et al.*, 2007).

Many studies have also been conducted linking nicotine with a variety of cancer types, including lung cancer (Brown *et al.*, 2012), breast cancer (Lee *et al.*, 2010), and colon cancer (Wong *et al.*, 2007), through α7 nAChR activation. Nicotine has been found to sustain the activation of mitogenic pathways, increase tumor growth, stimulate angiogenesis, and prevent apoptosis in many cancers, particularly lung cancer (Heeschen *et al.*, 2001; Zhu *et al.*, 2003). For example, nicotine was found to promote the progression of bronchioalveolar carcinoma cells (BACs), and plays a role in inducing these cells to be resistant to chemotherapy via inhibition of apoptosis. This inhibition was found to be due to the upregulation of anti-apoptotic proteins, such as inhibitor of apoptosis family of proteins (IAP) survivin and XIAP (Dasgupta *et al.*, 2006). Nicotine has also been found to phosphorylate (and therefore positively regulate) the anti-apoptotic proto-oncogene Bcl2 in human small cell lung carcinoma (SCLC) cells (Mai *et al.*, 2003).

Nicotine has been found to stimulate angiogenesis in mice through α7 nAChR activation (Heeschen *et al.*, 2001; Brown *et al.*, 2012). While many studies are looking at the effects of α7 nAChR activation in cancer development, α9 homopentamer nAChRs have also been found to play a role in breast cancer development. It was found that inhibition of the α9 receptor with siRNA inhibited cancer cell proliferation (Wu *et al.*, 2011), and nicotine-induced proliferating tumours were also found to express higher levels of α9 nAChRs than controls (Lee *et al.*, 2010). Interestingly, it was recently discovered that when MCF-7 breast cancer cells are treated with nicotine, they have higher numbers of CSCs compared to controls (Hirata *et al.*, 2010), and our lab confirmed this by discovering that treating MCF-7 breast cancer cells with nicotine in sphere-

forming conditions leads to an increase in sphere-forming cells over successive passages. Therefore, nAChR activation has been not only linked to cancer progression, but also to CSC self-renewal and proliferation.

Hypothesis

Based on both experimental evidence and existing literature, it is hypothesized that BTICs are particularly reliant on nAChR activation compared to their more differentiated progeny, and that inhibition of one or more of these receptors will lead to differentiation and/or death of TICs. Therefore, a potential breast cancer treatment would involve the use of a potent nAChR antagonist (to eliminate BTICs) and chemotherapy (to eliminate the bulk of the tumor population), thereby providing durable remission for breast cancer patients.

CHAPTER 2: MATERIALS AND METHODS

Cell Culture

All breast cancer cell lines were obtained from the American Type Culture Collection (ATCC) and propagated according to their specified protocols. Briefly, adherent cells were either cultured in Dulbecco's Modified Eagle Medium (DMEM) or Roswell Park Memorial Institute medium (RPMI) containing 10% fetal bovine serum (FBS), 1mg/mL fungizone, and 1% penicillin/streptomycin (all from Gibco). Cells were incubated at 37°C and 5% CO_2 in 75cm^2 or 150cm^2 flasks (Corning). Cells were grown to 70-90% confluency before being harvested using trypsin-EDTA (0.25%) (Life Technologies), and seeded in a new flask.

Adherent cell lines were also converted to non-adherent spheres by seeding 30 000- 120 000 cells/mL into stem cell medium (SCM) (low glucose DMEM: Ham's F-12 (3:1) supplemented with 1mg/mL fungizone, 1% penicillin/streptomycin (pen/strep), 2µg/mL B-27, 10ng/mL human bFGF, 20ng/mL human EGF, and 4ng/mL heparin [all from Invitrogen]), (Dontu *et al.*, 2003; Kurpios *et al.*, 2009, 2013; Kondratyev *et al.*, 2012). Sphere cultures were grown for 3-4 days before spheres were dissociated (by trypsin-EDTA and mechanical trituration), washed with Ham's F-12, and re-seeded in fresh SCM. Spheres derived from breast cancer cell lines were passaged twice before being used for experiments.

Sphere- and colony-forming assays

Sphere-forming assays were conducted using dissociated spheres (i.e. single cells) resuspended in human SCM, seeded in a 96-well plate (Corning), with 200µL of 30 000

viable cells/mL seeded (6000 cells) per well. Compounds of interest were most often diluted through two-fold dilutions of the stock concentration (usually 10μM) in 100% DMSO, Ethanol or water (where appropriate), and two microliters of decreasing concentrations of a given compound were then added (usually totalling 7 doses), as well as vehicle controls, in triplicate. Plates were incubated at 37°C for 4 days. Spheres were counted on day 4, and IC_{50} values were generated for each compound based on the percentage of spheres that were counted in the treated wells compared to control wells. Spheres were counted when they reached a size of 50μm in diameter (measured digitally using Openlab 3.1.4 software calibrated to 1 pixel= 1μm). The inhibitor concentration 50 (IC_{50}) for each compound was calculated using the GraphPad Prism 5™ software, with constrained nonlinear regression parameters log(inhibitor) vs. response – variable slope dose response curve.

Secondary sphere-forming assays involved single cells derived from dissociated spheres being treated in 25cm^2 flasks (Corning) for 4 days in the presence of the inhibitor or vehicle (in conjunction with a primary sphere-forming assay, as a control). Any spheres that formed were dissociated, and single viable cells were seeded in a 96-well plate at 6000 cells/well in fresh human SCM in the absence of any treatment. Spheres were then counted after 4 days. Sphere blocks were also created

Colony-forming assays were set up in concurrence with secondary sphere-forming assays, and involved the same treated, dissociated sphere-derived single cells from the 25cm^2 flasks, resuspended in adherent cell medium (Serum-containing RPMI, described previously). Ten-fold dilutions were used to obtain a culture of 300 cells/mL, and 1mL

was added to each 9.5cm^2 well of a 6-well plate (Corning) in triplicate for each pre-treatment. Plates were incubated for 10 days. Colony forming assays were also performed in HCC1954 cells grown in the presence of MG624. Briefly, HCC1954 adherent cells or single dispersed cells derived from HCC1954 spheres were seeded in a 6-well plate at 600 cells per well. Increasing concentrations of MG624 were added to the wells in triplicate, and plates were incubated for 10 days. Colonies were defined as 10 or more aggregated cells, and were counted using light microscopy.

PrestoBlue® cell viability assay

All PrestoBlue® experiments were completed using the Biomek3000 (Beckman Coulter) and a DTX880 multimode detector (Beckman Coulter). sphere-forming assays and PrestoBlue® assays were conducted on the same plates, on the same day for comparison of values, thus the compound dilution series (explained previously) remained the same for both assays. After spheres were counted on day 4 of incubation, 20µL of PrestoBlue® was added to each 200µL well (1:10 ratio), and PrestoBlue® reduction was read (530nM excitation / 590nM emission) after an additional 2 hours of incubation. Raw intensity values were converted to % residual activity using the following formula:

$$\%\, residual\ activity\ = \frac{Sample\ reading - Negative\ control}{Positive\ control - Negative\ control} \times 100\%$$

The IC_{50} of cell viability for each compound was calculated using GraphPad Prism 5™ software, similar to sphere-forming assay IC_{50} values (previously described).

Chemosynergy experiments

Chemosynergy experiments involved the use of HCC1954 breast cancer cells grown in sphere-forming conditions (explained previously). Single cells derived from

dissociated spheres were added to a 96-well plate, and treated with 2-fold dilutions of MG624 starting from 50µM down to 0.195µM to generate a robust IC_{50} curve. These doses were used alone, and in combination with 1 of 2 chemotherapeutics (taxotere or doxorubicin), at 1 of 2 doses each: 0.156µM or 0.078µM taxotere, or 0.0156µM or 0.0078µM doxorubicin. Plates were then incubated for 4 days, and spheres were counted on day 4. Sphere numbers were then converted to % sphere formation relative to the DMSO-only control, and expected percent sphere inhibition (%SphINH) was calculated based on the extent of sphere inhibition that would occur if the effect of the compounds were additive, using the equation:

$$Expected\ \%\ SphINH = \frac{\left(\begin{matrix}[\%SphINH\ at\ \ dose\ of\ MG624] \\ +[\%SphINH\ at\ dose\ of\ chemotherapy]\end{matrix}\right) - \left(\begin{matrix}[\%SphINH\ at\ dose\ of\ MG624] \\ \times\ [\%SphINH\ at\ dose\ of\ chemotherapy]\end{matrix}\right)}{100}$$

These values were calculated for all doses of MG624 in combination with each dose of either taxotere or doxorubicin.

Animal studies

All mouse experiments were performed with approval from and under the highest standards of the Canadian Council on Animal Care (CCAC), in a pathogen-free room with high-efficiency particulate air (HEPA)-filtered cages. Non-obese diabetic/severe combined immunodeficiency (NOD/SCID) mice were used for all experiments.

In order to establish subcutaneous tumors in either an *ex vivo* or *in vivo* assay, cells were suspended in a 1:1 mixture of phosphate-buffered saline (PBS) containing 5% FBS and Matrigel [BD Biosciences], and injected between the shoulders of 6-8 week old

female NOD/SCID mice (subcutaneously). Mice were palpated weekly to monitor for the presence of tumors.

There were two *ex vivo* assays conducted, both utilizing HCC1954 cells grown in sphere-forming conditions. In the first experiment, spheres were treated for 4 days with the IC_{90} of either MG624 or NDNI (both calculated to be 10µM), or the vehicle control (DMSO) before being dissociated, and 17 500 viable cells were injected into each mouse (10 mice per treatment). In the second *ex vivo* experiment, spheres were treated with one of three doses of MG624 (0.625µM, 3.5µM [the IC50] and 10µM) or DMSO, before being dissociated and 60 000 viable cells were injected into each mouse (5 mice per treatment).

In the *in vivo* experiment, 40 mice were injected with ~50 000 HCC1954 cells (grown in sphere-forming conditions) each. Once tumors reached $\geq 10mm^3$ (calculated by height, width, and length of tumor being measured using digimatic callipers (Mitutoyo), and multiplied), mice were randomly divided into 4 cohorts: A) Vehicle control, B) MG624 alone (20mg/kg, dissolved 1:1 100% ethanol [EtOH]:DMSO), C) taxotere alone (10mg/kg, dissolved in 100% ethanol), and D) MG624 + taxotere (20mg/kg MG624, 10mg/kg taxotere). Mice were treated via intraperitoneal (IP) injections. MG624 (or vehicle) was injected once per day for 5 days, followed by 2 days off, for 3 weeks. Taxotere (or vehicle) was administered once per week. Mice only received one injection on any given day. The injection mixture at the start of each treatment cycle consisted of one part 10X taxotere (or 100% EtOH), six parts water, two parts 5X MG624 (or 1:1

100% EtOH:DMSO) and one part Tween 20. On all other treatment days, the taxotere/100% EtOH fraction was replaced by water.

At the end of the treatment period, 3 days after the last dose of MG624, tumor volumes were measured one last time before mice were sacrified and tumor tissue was removed and processed for analyses. Four mice from the taxotere cohort and four mice from the MG624 + taxotere cohort whose tumors had either completely or nearly completely regressed were monitored for up to 22 weeks for tumor recurrence/progression.

Propagation of patient-derived xenograft tumor cells in vitro

Primary patient tumor samples were obtained by Kay Dias (Dr. Anita Bane's lab) from Dr. Peter Lovrics from St. Joseph's Healthcare Hamilton (Hamilton Health Sciences), and were processed and injected orthotopically into NOD/SCID/γ (NSG) mice by Craig Aarts (Dr. John Hassell's lab). The patient-derived xenografts (PDXs), designated as generation 1 (G1), that arose were harvested, processed and injected into new NSG mice. PDXs used in my experiments were G2 and G3 X81 PDXs. X81 is estrogen receptor positive (ER+), progesterone receptor negative (PR-) and human epidermal growth factor receptor 2 negative (HER2-), designating it as luminal B subtype (based on gene expression profiling and immunohistochemistry).

In order to obtain single cells from X81 PDXs, fresh xenograft tumors were harvested from NSG mice, and mechanically minced for 10 minutes before being enzymatically digested with a cocktail of DMEM supplemented with 2% FBS, 1mg/mL fungizone, 1% pen/strep, 3mg/mL collagenase A (Roche Diagnostics) and 4% trypsin (all

filtered through a 0.45µm syringe filter [Fisher Scientific]) for 30 minutes. Cells were then filtered through a 40µm Falcon™ cell strainer (Fisher Scientific), and centrifuged at 1000rpm for 15 minutes. Cells were washed once with Ham's F-12 medium, and resuspended in human SCM. Cells were then counted using trypan blue, and 100 000 cells/mL were seeded into flasks (or 96-well plates) for sphere-forming assays, previously described (Kurpios *et al.*, 2009). X81 sphere-forming assays were incubated for 7 days (instead of 4 days), as PDX spheres require a longer period of time to grow.

Treated sphere blocks

Sphere blocks were created using HCC1954 cells grown in sphere-forming conditions for 2 passages to establish spheres. Spheres were then dissociated, and seeded at a density of 30 000 cells/mL in T150 flasks. Flasks were incubated for 4 days to allow spheres to grow and establish before 10µM of MG624 was added (or equal volume DMSO) to the media. Spheres were exposed to either treatment for 48 hours, before being centrifuged at 500rpm for 5 minutes. The supernatant was then removed, and spheres were resuspended in formalin. Spheres were fixed for 15 minutes before agar was added at a 1:1 ratio. The formalin-agar-sphere suspension was then immediately transferred to a 1.5mL eppendorf tube, prepared previously with the conical bottom being replaced by parafilm. After 20 minutes of incubation on ice, sphere blocks were then transferred to a tissue cassette and placed in formalin for 48 hours before being sent to histology for sectioning.

X81 sphere blocks were prepared similarly, however they were grown in sphere-forming conditions upon cell isolation from a 3rd generation tumor freshly isolated from

an NSG mouse. X81 spheres were grown at a density of 100 000 cells/mL, and were incubated for 7 days before the 48 hour treatment. For X81 spheres, two doses of MG624 were used: 5μMand 10μM.

Histology, immunofluorescence and immunohistochemistry

Harvested tumors were fixed in 4% paraformaldehyde, embedded in paraffin, and sectioned into 5μm sections (Kurpios *et al.,* 2009). Tumor sections and sphere blocks were all stained with hematoxylin and eosin (H&E). Slides were dewaxed in xylenes, and antigen retrieval was conducted using Vector Antigen Unmasking Solution (Vector lab), and slides were blocked with 3% normal goat serum (NGS) in PBST (PBS with 0.03% Tween-20) for 45 minutes. Primary antibodies were diluted in 3% NGS in PBST and added to slides for 1 hour at room temperature. Slides were washed three times for five minutes with PBST and incubated with the secondary antibody (all diluted 1:200) conjugated to goat anti-mouse Alexafluor 488 (Invitrogen) or goat anti-rat Alexafluor 568 (Invitrogen) for 1 hour at room temperature. Nuclei were visualized using 4', 6'-diamidino-2-phenylindole (DAPI) fluorescent stain in Vectashield mounting medium (Vector Laboratories), and staining was analysed using an inverted fluorescence microscope (Leica), with images being captured using Improvision Openlab software. Primary antibodies and dilutions were as follows: CK8 – polyclonal rat anti-human (in-house hybridoma) 1/8, αSMA- monoclonal mouse anti-human (Sigma) 1/750, αSMA-monoclonal rabbit anti-human (Abcam) 1/100, Human mitochondria (HuMt): monoclonal mouse anti-human (Antibodies-Online) 1/500. TUNEL staining was carried out as per manufacturer's protocol (Millipore). Immunohistochemistry (IHC) was performed as

previously described (Pechoux *et al.*, 1999). Briefly, tumor sections were stained for CK5 (1:130 dilution) and Ki67 (1:100 dilution). Antigen retrieval was carried out in a Micromed T/T Mega Microwave Processing Lab Station (ESBE Scientific, Markham, Ontario, Canada) and sections were developed with diaminobenzidine tetrahydrochloride (DAB) and counterstained in Mayer's hematoxylin.

Statistical analyses

Sphere-forming assay curves are displayed as the means of at least 3 technical replicates ± standard error mean (SEM). Bar graphs are displayed as means of at least 3 technical replicates ± standard deviation (SD) unless otherwise stated. The significance of all data was calculated using GraphPad Prism 5™ software, or the Microsoft Excel data analysis tool, where statistical significance = $p < 0.05$. The significance of the survival curve comparisons in both *ex vivo* assays (tumor-free survival) and in the *in vivo* "relapse" experiment (% tumor progression-free survival) was determined using the Log-rank (Mantel-Cox) Test. The significance of the difference in secondary sphere size post-treatment with proadifen, NDNI and dicyclomine, as well as the significance of the *in vivo* data (comparison of tumor volumes at end of treatment), and significance of the TUNEL assay (% TUNEL-positive nuclei) and Ki-67 staining (% Ki-67 positive nuclei) for the *in vivo* experiment tumor sections, was determined using a one-way analysis of variance (ANOVA) followed by a Tukey's Multiple Comparison Test to determine which groups were considered significantly different. The significance of the TUNEL assay used to compare TUNEL-positive nuclei in treated sphere block sections was calculated using a student's t-test.

CHAPTER 3: RESULTS

Identifying nAChR antagonists that inhibit sphere formation

A pharmaceutical approach was used in attempt to identify the nAChR likely responsible for BTIC self-renewal and proliferation. A chemical sphere-forming assay screen was performed in MCF7 cells, which are known to be an enriched, sustainable source of sphere-forming cells when grown as tumorspheres (Dontu *et al.*, 2003; Ponti *et al.*, 2005). PrestoBlue® was also used in follow up assays to examine the differences between sphere numbers, cell proliferation and cytotoxicity. PrestoBlue® is similar to the commonly used alamarBlue™ reagent, which is used to study the ability of cells to reduce a nonfluorescent compound (resazurin) to a fluorescent molecule (resorufin) a measure of cell metabolism (and indirectly, cell proliferation) via fluorescence readings.

In total, 15 nAChR antagonists and 3 mAChR antagonists were tested in sphere-forming assays at 8 different concentrations (including the vehicle control), and IC_{50} values were generated using GraphPad Prism 5 software (Table 1). Of these 18 compounds, 9 inhibited sphere formation (Figure 2), and the other 9 compounds appeared to have little to no effect (Appendix 1). Any compound that showed minimal to no effect on sphere formation at 250μM was considered inactive (i.e. not binding to the nAChR responsible for sphere-forming cell survival).

Adiphenine, as well as its more potent analog proadifen, are cited as being non-competitive nAChR antagonists, with relatively high affinities for α1β1δγ, α3β4, α4β2, α4β4 (Gentry & Lukas, 2001), therefore they could be considered fairly non-specific for α

nAChRs. However, the activity of proadifen and adiphenine were not tested against any other nAChR subunit complexes, thus the nAChR subunit(s) they may be signaling through may not be any of the aforementioned combinations. MG624 is highly selective for α7, and it has a relatively low (μM) affinity for α4β2 (Gotti *et al.*, 1998). Once again, this compound was not tested for its affinity for many other possible nAChR subunit combinations, limiting our ability to identify any receptors that are selectively being targeted by many these compounds. NDNI has been found to have a high affinity for α4β2 (Wilkins *et al.*, 2003), some affinity for α3α6β2, and a low affinity for α7 (Sumithran *et al.*, 2005), however it was only tested against these 3 receptors.

Dicyclomine, the one mAChR antagonist (out of 6) that was previously found to successfully chemosensitize breast cancer cells, potently inhibited sphere-formation. Dicyclomine has a high affinity for M1 and M3 receptors, but a low affinity for M2 receptors (Jiang *et al.*, 2000). However, α9 receptors have been found to display both muscarinic and nicotinic receptor properties, and many mAChR antagonists and agonists have been found to show high affinities towards α9 (Verbitsky *et al.*, 2000), thus dicyclomine may actually be binding to α9, however this has not yet been tested.

Lobeline was found to inhibit sphere formation, however it has a high IC_{50} of 60.03μM, making it very possible that it is non-specifically targeting a receptor other than the one it has been cited to target, i.e. α4β2 (Hillmer *et al.*, 2013). SR 16584 is an α3β4 nAChR antagonist (IC_{50} = 10.2μM), and has been found to show minimal to no affinity towards α4β2 and α7 (Zaveri *et al.*, 2011). SR 16584 was found to have a high IC_{50} (i.e. 129.1μM), indicating it may actually be functioning through either α4β2, α7 or was

simply toxic to cells at such a high concentration. Memantine had the highest IC_{50} among all active compounds and it has been found to target many different receptors, including α7 (Aracava *et al.*, 2005), and α4β2 (Buisson & Bertrand, 1998). However, memantine is also a low-affinity noncompetitive antagonist of NMDA receptors (Chen & Lipton, 2006), thus its molecular target cannot be inferred. Of the six most potent nAChR antagonists tested, 3 have been reported to target α4β2 (i.e. NDNI, MG624 and Lobeline); however, numerous inactive compounds were also found to target this receptor. It is possible that the nAChR required for sphere formation has not yet been tested.

The molecular structures for the 4 most successful sphere inhibiting compounds with an IC_{50} below 10μM can be found in Table 2. Of the four most potent antagonists, only proadifen and dicyclomine share similar structures, indicating that these compounds are most likely binding to AChRs, instead of binding to an unknown target and functioning through some other unrelated mechanism.

There were also many compounds that had no effect on sphere formation. These included: mecamylamine, an antagonist of α4β2 (Fedorov *et al.*, 2009), α4β4 and α2β4 (Chavez-noriega *et al.*, 1997); strychnine, a known α9 and α7 antagonist (Elgoyhen *et al.*, 2001) and a noncompetitive antagonist at α4β2 (Matsubayashi *et al.*, 1998); tubocurarine and atropine, both of which are α9 antagonists (Elgoyhen *et al.*, 2001), however tubocurarine also targets α7 and α3β2 (Chavez-noriega *et al.*, 1997) and atropine primarily targets muscarinic receptors (Lenzken *et al.*, 2007); Dihydro-β-erythrodine targets α4β2 and α4β4 receptors (Chavez-noriega *et al.*, 1997); methyllycaconitine, a potent α7 antagonist, has also been found to also interact with

various combinations of α3/α6/β2/β3 receptors (Mogg *et al.*, 2002); 5-Iodo-A-85380 is highly selective for α4β2 receptors (Mukhin *et al.*, 2000); and finally scopolomine, an M1 mAChR antagonist, which has also been found to antagonize NMDA receptors (Falsafi *et al.*, 2012). Again, as previously mentioned, most of these compounds have only been tested for their affinity for 2 or 3 receptors, and none of them have been tested against all nAChRs.

One interesting finding was that α-Bungarotoxin, a potent α9 and α7 antagonist (Johnson *et al.*, 1995; Elgoyhen *et al.*, 2001), did not inhibit sphere formation, possibly indicating that the receptor(s) likely responsible for sphere-forming cell self-renewal and proliferation are non-αBgtx-nAChRs, which are heteromeric in nature, made up of α2-α6, and β2-β4 subunits (Gotti & Clementi, 2004). Alternatively, it is possible that α-Bungarotoxin was inactive in our system; to avoid denaturing the proteins, however, α-Bungarotoxin was dissolved in PBS, as per published methods (Lenzken *et al.*, 2007), on ice, over a 2-hour time period, and mixed using a wide bore tip, and gentle trituration.

Following sphere-forming assays, PrestoBlue® assays were also performed for all 8 of the compounds found to inhibit sphere formation, as well as 2 of the inactive compounds. The rationale behind this experiment was to confirm that the spheres that formed were indeed comprised of viable cells, and to somewhat validate sphere-forming assay data (Appendix 2). These assays correlated with the sphere-forming assays, however for two of the most potent compounds tested (MG624 and NDNI) a residual ~20% fluorescence could reproducibly be detected in these wells, even at doses beyond the concentration found to completely inhibit sphere formation. This could indicate that

these compounds actually did selectively target sphere-forming cells, and not their differentiated progeny; thus the descendants of sphere-forming cells could be responsible for the metabolic activity being detected in these wells.

Primary sphere-forming assays for the four most potent antagonists were also carried out in HCC1954 breast cancer cells, and yielded similar IC_{50} values (Figure 3A). HCC1954 cells are a more chemoresistant cell line than MCF7 cells (Hallett, 2012), and are more useful for tumorigenesis studies as they form consistent, rapidly proliferating tumors when injected into NOD/SCID mice. Thus, subsequent *in vitro* analyses focused on using the HCC1954 cell line.

Secondary Sphere-Forming Assays

To determine whether the antagonists functioned by a reversible or irreversible mechanism, we performed secondary sphere-forming assays. Using increasing concentrations of the four most potent compounds, secondary sphere-forming assays were also performed (Figure 3B). Secondary sphere-forming assays involve spheres being treated for 4 days in the presence of the inhibitor or vehicle, and any spheres that form are dissociated, and single viable cells are seeded into a 96-well plate in the absence of any inhibitor. In addition to determining the irreversibility of a compound, secondary sphere-forming assays also show that an inhibitor is targeting the sphere-forming cell, as a compound may be only targeting the descendants of sphere-forming cells making up the majority of a sphere, resulting in single cells being observed. However, when these cells are seeded into a secondary sphere-forming assay, spheres would form in the absence of

the inhibitor, as the sphere-forming cells would not have been targeted by the compound, and would maintain their sphere initiating capability. If a compound targets sphere-forming cells specifically, then when single cells are seeded into a secondary sphere-forming assay, spheres will not form due to the lack of sphere-forming cells.

NDNI, proadifen and MG624 all inhibited secondary sphere formation, indicating that these compounds are indeed irreversible. On the other hand, while dicyclomine reduced primary sphere formation to values 54% and 18% of the control in spheres treated with 6.25μM and 12.5μM, its effect was reversible. This indicates that dicyclomine either targeted the progeny of sphere-forming cells, or that the effects of dicyclomine on sphere-forming cells is reversible. Pictures were also taken for primary and secondary sphere-forming assays (Appendix 3). Of the 3 irreversible compounds tested (NDNI, proadifen and MG624), MG624 was found to show the greatest specificity for sphere-forming cells. In the primary sphere-forming assay for MG624, sphere formation was reduced by 20%, 40%, 50%, and 99% at 1.25μM, 2.5μM, 5μM and 10μM, respectively, and the appearance of the spheres in treated wells appeared dark, accompanied by what appeared to be cell death around them (Appendix 3). Interestingly, in the secondary sphere-forming assay, there were no spheres that formed at any of the concentrations. This indicates that MG624 may be selectively targeting sphere-forming cells compared to NDNI, proadifen, and dicyclomine, and that this effect is irreversible. Primary and secondary sphere-forming assays were all conducted at least 3 times, with 3 technical replicates per experiment.

Next, all secondary spheres located in the two or three most sphere-dense sections of each treatment well (in triplicate) were measured digitally using Openlab 3.1.4 software

calibrated to 1 pixel= 1μm (Figure 3C). It was found that as the concentration of NDNI, proadifen and dicyclomine increased in the primary sphere-forming assay, secondary sphere size decreased (ANOVA p-values were 6.70×10^{-08}, $2.3 \times 10^{-13,}$ and 0.00032, respectively). This suggests a reduction in cell proliferation or an increase in cell death during secondary sphere formation. Figure 3C (bottom) demonstrates the lack of secondary spheres after HCC1954 cells were treated with 1.25μM MG624.

Interestingly, MG624 (a selective α7 nAChR antagonist) has been found to show anti-tumourigenic properties in mice, by inhibiting human microvascular endothelial cell (HMEC) proliferation and nicotine-induced angiogenesis in human small cell lung carcinoma (SCLC) cells (Brown *et al.*, 2012). In this study, MG624 was fed to male nude mice, 50mg MG624/kg food (roughly 10mg MG624/kg body weight of mouse per day) for 19 days, without causing any discomfort, toxicity or changes in the eating/drinking habits of the mice, demonstrating that MG624 is a safe compound to be used *in vivo*. Additionally, due to its exceptional sphere-forming cell-specificity, MG624 is also the most promising candidate for further sphere-forming cell/TIC-related experiments.

Elucidating the specificity of MG624 for sphere-forming cells over other cells in vitro

Among the four most potent nAChR antagonists, MG624 was found to completely inhibit secondary sphere formation at concentrations that displayed only minimal inhibition of sphere-formation (i.e. 3.125μM) in the primary sphere-forming assay. The latter could indicate that MG624 specifically targeted sphere-forming cells, possibly through a self-renewal pathway (Zeng *et al.*, 2013). Therefore dramatic differences seen between the frequency of sphere formation in a primary versus a secondary sphere-

forming assay may be indicative of MG624 interfering with the self-renewal of sphere-forming cells. Therefore, in order to fully elucidate the nature of this specificity, we wanted to test lower doses of MG624 in a primary and secondary sphere forming assay starting with doses that would have no effect on primary sphere formation, yet would completely inhibit secondary sphere formation. The hypothesis for this experiment was that MG624 inhibits secondary sphere formation in a dose-dependent manner. Therefore we performed 2-fold dilutions of MG624 in HCC1954 cells grown in sphere-forming conditions, from 0.63µM to 0.03µM, and used these 10 concentrations to seed both a primary and secondary sphere-forming assay (Figure 4A). None of the concentrations tested had any effect on sphere formation in the primary sphere-forming assay, however once MG624 was removed, the secondary sphere-forming assay revealed a similar dose-dependent decrease in sphere frequency that was seen in the primary sphere-forming assay, at >30-fold lower concentrations of MG624. We then plotted these values in a log inhibitor vs. % sphere formation graph to generate a secondary "residual IC_{50}" (Figure 4B), which demonstrates the concentration of MG624 required to irreversibly inhibit the formation of 50% of secondary spheres (compared to the control), and compared this curve to the actual IC_{50} curve for MG624 in a primary sphere-forming assay. The secondary "residual IC_{50}" suggests that MG624 has a higher specificity for sphere-forming cells over all cells *in vitro*. These data were reproduced in one additional independent biological experiment. Spheres that formed at doses that had virtually no effect on primary sphere formation, but completely abolished secondary sphere formation, were often surrounded by an envelope of what appeared to be dead cells

(Figure 4C). Aside from demonstrating that these spheres are phenotypically different than control spheres, this could reflect the sphere's limited growth potential once the sphere-forming cell is eliminated.

Previously, we found that cells treated with MG624 still display residual metabolic activity in a PrestoBlue® assay in wells that did not contain spheres, but did contain dispersed individual cells (Appendix 2). These single cells can be visualized in Figure 4C. Therefore, we wanted to determine whether or not these cells are viable, and if so, whether they could form colonies as a read out of the proliferative capability of the remaining, dispersed individual cells (Figure 4D). In this experiment, HCC1954 cells were treated with MG624 for 4 days in sphere-forming conditions, spheres were dissociated, and 600 viable cells were seeded into a 6-well plate. Secondary sphere-forming assays were also run in parallel as a control. Interestingly, colonies arose at concentrations of MG624 that completely inhibited secondary sphere formation. However, the effect of MG624 primary sphere treatment on the ability of treated cells to form colonies was still dose-dependent, indicating that MG624 does indeed target non-sphere-forming cells, however the specificity is less than that of the specificity of MG624 toward sphere-forming cells, thus higher doses of MG624 are needed to inhibit colony-formation post-MG624 treatment.

Additionally, colony forming assays were conducted in the presence of MG624 in order to elucidate the specificity for breast cancer progenitor cells (colony-forming cells) compared to sphere-forming cells, and viable, further differentiated cells. For this experiment, adherent HCC1954 cells and single dispersed HCC1954 cells derived from

spheres were plated at 600 cells per well in a 6 well plate, and increasing concentrations of MG624 were added to the wells (Appendix 4). It was found that adherent HCC1954 cells have a higher percentage of colony-forming cells than spheres (58% compared to 23%). It was also found that the IC_{50} for MG624 was essentially equal in both cell populations in a colony forming assay, indicating that independent of the source or percentage of colony-forming cells in a cell population, MG624 has a predictable potency. This explanation depends on the assumption that there are specific cells within a pool of adherent cells or single, dispersed sphere-derived cells capable of colony formation, but not sphere-formation. Alternatively, these data could indicate that the stress placed on single cells derived from spheres during sphere dissociation (manual trituration and enzymatic digestion), results in a lower % sphere-forming efficiency. The IC_{50} between sphere-forming assays and colony forming assays cannot be properly compared due to the difference in assay incubation time (4 days compared to 10 days) and difference in medium supplements, etc. However, the colony-forming assay IC_{50} was found to be lower than a primary sphere-forming assay IC_{50}, but higher than the secondary sphere-forming assay "residual IC_{50}".

Testing MG624 in sphere-forming assays across a panel of cell lines and one PDX

In order to determine whether MG624 selectively effected the sphere-forming activity of breast tumor cell lines representative of other particular breast cancer molecular subtypes we tested its activity in multiple cell lines. To this end, MG624 was tested in one basal cell line (HCC1954), 5 luminal cell lines (MDA-MB-453, BT-474, MCF-7, ZR751, T47D), and one luminal B PDX X81 (G3). All cells were grown in non-

adherent sphere-forming conditions, and were used in both primary and secondary sphere-forming assays (Figure 5). The corresponding IC_{50} curves generated from GraphPad Prism5 software can be found in Figure 5A, and IC_{50} values are shown in Table 3. Whereas some cell lines were found to be slightly more sensitive to MG624 (MDA-MB-453 cells and T47D cells), and others were found to be somewhat more resistant (BT-474 cells and ZR751 cells) compared to HCC1954 cells, overall MG624 consistently inhibited sphere-formation in all cell lines, indicating that it has little molecular subtype specificity.

Three cell lines, other than the already-tested HCC1954 cells (BT-474, MCF-7, and ZR751), and the PDX X81-derived cells were then used in secondary sphere-forming assays to assess whether the phenomenon observed in HCC1954 spheres might be observed in other cell lines, namely the vast difference between primary and secondary sphere forming frequencies (Figure 5B). BT-474 cells showed a similar trend to HCC1954 cells, as concentrations of MG624 found to have no effect on primary sphere formation (0.625μM and 1.25μM), secondary sphere formation was greatly affected (~95% and 97% reduction in sphere formation, respectively). On the other hand, MCF-7 and ZR751 cells were more resistant in a secondary sphere-forming assay compared to HCC1954 and BT474 cells, in that the concentration of MG624 required to completely inhibit secondary sphere formation was greater than the IC_{50} for both compounds. However, these cell lines still followed a similar trend: estimated secondary "residual IC_{50}" values were consistently at least 10-fold lower than primary IC_{50} values in all cell lines (Table 3).

Importantly, the PDX X81 cells displayed a very similar trend, a dose-dependent decrease in primary spheres and a more dramatic decrease in secondary spheres, with the dose of 0.3125µM MG624 leading to ~40% reduction in spheres in the primary sphere-forming assay, and a 75% reduction in spheres in the secondary sphere-forming assay. Figure 5C contains images of X81 primary and secondary spheres treated with either DMSO or 2.5µM MG624. Overall, secondary X81 spheres were much smaller after being passaged even one time, as PDX cells cannot usually be propagated in culture for more than 2 passages. However trends can still be seen: even at 2.5µM (half of the IC_{50} for MG624 in X81 cells) spheres appear smaller, they tend to cluster together, and when passaged and seeded in the absence of MG624, no spheres form after being treated with this concentration or even a 2-fold lower concentration (1.25µM).

Ex vivo transplantation of cells treated with nAChR antagonists into NOD/SCID mice

An *ex vivo* assay can be used to demonstrate whether a compound targets functional TICs. While sphere-forming cells and TICs both contain markers of, and share similar properties to CSCs, not every sphere-forming cell is a TIC (Grimshaw *et al.*, 2008). Spheres have been found to be enriched for cells containing CSC surface markers such as $CD44^{+}/CD24^{-/low}$, and when cells are sorted via flow cytometry based on these surface markers, the frequency of CSC surface markers such as $CD44^{+}/CD24^{-/low}$ in a cell population does not necessarily correlate with tumorigenicity, i.e. having a higher percentage of $CD44^{+}/CD24^{-/low}$ cells in one cell line compared to another does not mean that cell line will initiate more tumors, or that those tumors will grow more rapidly

(Fillmore & Kuperwasser, 2008). Thus a sphere-forming cell is not entirely analogous to a TIC, and while sphere-forming cells are a useful in vitro target, sphere-forming cell frequency does not accurately predict TIC frequency (Pastrana *et al.*, 2011). Hence, an *ex vivo* assay complements, and in many ways verifies, sphere-forming assay data. Therefore, the most potent, irreversible compounds that successfully inhibited both primary and secondary sphere formation were then used to treat HCC1954 spheres for a transplantation experiment into NOD/SCID mice.

These compounds included MG624 and NDNI (Figure 6 A-C). In this experiment, spheres were treated for 4 days with the IC_{90} of either MG624 or NDNI (both calculated to be 10μM) before being dissociated, and equal numbers of dispersed, viable cells injected into mice. Primary and secondary sphere-forming assays were also set up as controls (Figure 6A), revealing similar results to what would be expected from both of these compounds. Mice were then monitored weekly (by palpation) for the appearance of tumors. In this experiment half of the control mice developed palpable tumors 5 weeks post-injection; all the remaining mice developed tumors 2 weeks later.

After 7 weeks post-injection, 2 mice injected with NDNI-treated HCC1954 cells developed palpable tumors, and one mouse per week succumbed to tumors until week 10, when no other mice developed tumors; the remaining 5 tumor-free mice were sacrificed after 12 weeks had elapsed post tumor cell injection (Figure 6B).

In the cohort of mice injected with MG624-treated HCC1954 cells, one mouse developed a palpable tumor after 7 weeks, one at 8 weeks, and a third mouse developed a palpable tumor after 11 weeks. The remaining 7 mice remained tumor free and were

sacrificed after 12 weeks post-injection (Figure 6C). Both MG624 and NDNI treatments of HCC1954 cells were found to significantly delay tumor formation (p-value <0.0001), indicating that both of these compounds targeted functional TICs. However, the IC_{90} of MG624 was used in this experiment, when it has been shown *in vitro* that MG624 can inhibit secondary sphere-formation at doses that do not inhibit primary sphere-formation at all.

To determine whether we could reproduce the aforementioned data, we performed a second *ex vivo* experiment using HCC1954 cells grown in sphere-forming conditions, and treated with 3 different doses of MG624 (0.625µM, 3.5µM, and 10µM) or the vehicle control (DMSO). Five mice per cohort were injected with 60 000 viable cells each, and mice were palpated for tumors weekly. The results of the sphere-forming assays are shown in Figure 5D. After 4 weeks, 4 of 5 vehicle-treated mice, and 2 of 5 mice injected with HCC1954 cells treated with 0.625µM of MG624 developed palpable tumors. One week later, all of the control mice had succumbed to tumors, as well as 2 more mice from the 0.625µM MG624-treated cohort. The remaining mouse from this cohort was tumor-free until week 8. The slight delay observed in tumor formation in this cohort was not statistically significant, indicating that while secondary spheres were completely abolished at this concentration of MG624, functional TICs were still resident in this tumor cell population. Remarkably, the IC_{50} dose of 3.5µM MG624 was able to significantly delay tumor formation; one mouse developed a palpable tumor after 6 weeks, two at 8 weeks, one more at 10 weeks, and the remaining mouse at 11 weeks (p-value of 0.0016). Similar to the first *ex vivo* experiment, treating HCC1954 cells grown in

sphere-forming conditions with 10µM MG624 resulted in only one mouse (out of 5) with a palpable tumor by week 9 (p-value= 0.0016). All mice were sacrificed 11 weeks after injecting them with the tumor cells. These assays demonstrate that both NDNI and MG624 specifically target TICs as defined by the "gold standard" functional assay for such tumor cells.

Determining if MG624 synergizes with chemotherapy in vitro

Before testing any compounds *in vivo*, we wanted to determine whether they could be combined with chemotherapy *in vitro* to produce a synergistic effect in a sphere-forming assay. The hypothesis for this experiment is that nAChR antagonists could specifically target sphere-forming cells, and the chemotherapeutic could eliminate the remaining cells within the sphere, resulting in a greater reduction in sphere formation than either treatment alone. We opted to use only MG624 for this experiment. To this end, a sphere-forming assay was set up involving 2-fold dilutions of MG624 starting from 50µM down to 0.195µM to generate a robust IC_{50} curve. These doses were used alone, and in combination with each of 2 chemotherapeutics, at 1 of 2 concentrations: 0.156µM or 0.078µM taxotere, or 0.0156µM or 0.0078µM doxorubicin. These concentrations were chosen based on the IC_{50} curves previously generated in our lab for these drugs, with the intention of choosing concentrations with only a minor effect on sphere-formation on their own. If specific concentrations of two different compounds dramatically inhibit sphere formation on their own, combining them together will not be as dramatic as combining specific concentrations of 2 compounds that have little to no effect on sphere formation on their own, but synergize together to inhibit sphere formation. Therefore, the

~IC_5 and ~IC_{10} of taxotere or doxorubicin were used (Figure 7). The expected % sphere inhibition was calculated for each combination of MG624 and chemotherapy concentrations based on the effect of these doses alone on sphere formation, and the expected sphere inhibition if these compounds functioned additively. A heat map was then generated (Figure 7A) demonstrating which concentrations of both treatments produced expected results (i.e. additive, yellow), which doses produced a lesser effect than what should be expected (i.e. masking effect, blue), and which concentrations induced greater sphere inhibition than would be expected from both compounds had their effects been additive (i.e. synergy, red). This heat map revealed that MG624 showed the greatest synergy around its IC_{50} (3.5µM) with 0.156µM taxotere, and at 1.56µM MG624 combined with 0.0078µM doxorubicin.

The areas with the greatest synergy were then used to generate expected vs. actual IC_{50} curves for MG624 combined with either chemotherapeutic. This involved adding the effect of chemotherapy alone to the effect of MG624 alone at each concentration, generating expected values (Figure 7B, red curves). The actual IC_{50} curves generated for MG624 alone (blue) and MG624 in combination with taxotere or doxorubicin (green) were then compared to the expected curve. The expected curves overlap the curves generated from the effect of MG624 alone because the effect of taxotere or doxorubicin alone on sphere-formation at the concentrations chosen was negligible, thus the additive effect of either chemotherapeutic and MG624 would not appear noticeably different than MG624 alone. The effect of chemotherapy alone has been removed from the IC_{50} curves generated from the observed sphere formation for MG624 in combination with

chemotherapy, therefore any difference observed between the expected (red) sphere inhibition and the actual sphere inhibition (green) would indicate that synergy has taken place at those doses. These curves revealed that the most MG624/chemo synergy took place at 0.156μM taxotere, and 0.0078μM doxorubicin, which correlates with the heat map.

Using doses of MG624 that showed the most synergy with a specific dose of chemotherapy, bar graphs were also generated to show the actual vs. expected (additive) effect of MG624 and either taxotere or doxorubicin, compared to DMSO alone, taxotere/doxorubicin alone, and MG624 alone (Figure 7C). The dotted line represents the expected % sphere formation that should be observed if the effects of MG624 and chemotherapy on sphere formation were additive. MG624 and taxotere once again appear to synergize at 3.125μM MG624 and 0.156μM taxotere (p-value < 0.0001), and MG624 and doxorubicin appear to synergize at 1.56μM MG624 and 0.0078μM doxorubicin (p-value < 0.0002). Therefore, it is possible that MG624 and chemotherapy may synergize *in vivo* to shrink tumors, similarly to how they synergize to inhibit sphere formation.

Treatment of tumor-bearing mice with MG624 alone and in combination with taxotere

In order to determine the effect of MG624 tumor growth, an *in vivo* experiment was conducted. In this experiment 40 mice were injected with HCC1954 cells (grown in sphere-forming conditions). Thereafter the mice were palpated for tumors weekly (Figure 8A). When tumors achieved a volume of $\geq 10mm^3$, the mice were randomly divided into 4 cohorts: A) Vehicle control, B) MG624 alone (20mg/kg, dissolved 1:1 100%

ethanol:DMSO), C) taxotere alone (10mg/kg, dissolved in 100% ethanol), and D) MG624 + taxotere (20mg/kg MG624, 10mg/kg taxotere).

The dose of MG624 used was chosen based on a maximum tolerated dose (MTD) experiment conducted in our lab, as well as a published dosing regimen of MG624 administered to mice orally with no negative health consequences (Brown *et al.*, 2012). The dosing regimen for taxotere was chosen based on published therapeutically successful taxotere dosing regimens found to have an effect on tumor growth, with limited morbidity in mice (Granda *et al.*, 2001; Hotchkiss *et al.*, 2002; Takebe *et al.*, 2011; Korkaya *et al.*, 2012). Taxotere was chosen over other chemotherapies because it has been successfully used in our lab for *in vivo* studies in NOD/SCID mice, results in less negative health effects in patients compared to doxorubicin (which has been found to cause cardiac toxicity and cardiomyopathy) (Misset *et al.*, 1999; Shi *et al.*, 2011), and successfully synergized with MG624 *in vitro*, with a lower p-value than doxorubicin.

Mice were treated via intraperitoneal (IP) injections. MG624 (or vehicle) was injected once per day for 5 days, followed by 2 days off, for 3 weeks. Taxotere (or vehicle) was administered once per week. Tumors were measured using calipers at the beginning of each weekly treatment regimen. Mean tumor volumes for each cohort are shown in Figure 8B. The control group demonstrated exponential tumor growth from the start of treatment, as would be expected, as tumor volumes follow a linear trend and the y-axis of this graph is the $\log^{10}$ of tumor volumes. The MG624-treated cohort followed a similar trend, however tumor growth was delayed by one week. The significance of this delay is unknown, however it could be speculated that MG624 had an initial effect on the

tumor when it was small, but was ultimately unable to prevent the exponential growth of the tumor, which would mostly be made up of the progeny of TICs. We have shown that MG624 has a higher specificity for sphere-forming cells over other cells *in vitro,* and this specificity may also be occurring *in vivo*. By the end of treatment, all MG624-treated mice developed tumors comparable in volume to control tumors. As would be expected from the taxotere-treated cohort, the mean tumor growth rate was reduced, with only a slight increase in mean tumor volume between the start and end of the treatment regimen. The combination treatment of MG624 and taxotere initially reduced tumor growth for 1 week and caused tumors to shrink by the second and third weeks. Tumor volumes at the end of the treatment cycle are shown in Figure 8C. The taxotere and combination cohorts both had significantly lower mean tumor volumes at the end of the treatment regimen; however, tumor volumes in the taxotere cohort were similar to starting tumor volumes (average 22mm^3), whereas the combination of MG624 and taxotere actually shrank all tumors, and 4 of the 7 mice were tumor-free at the end of the treatment regimen.

At the end of the treatment regimen, all mice were sacrificed, and 2 tumor samples per cohort were prepared for sectioning. Four mice from the taxotere-treated cohort (tumor volumes: 1, 2, 8 and 18mm^3) and 4 mice from the combination-treatment cohort (all tumor-free) were not sacrificed, and were instead monitored weekly for tumor relapse/progression, to determine the long-term effect of both treatments on tumor recurrence (Figure 8D). After 2 weeks of follow up, all 4 taxotere-treated mice experienced tumor recurrence/progression whereas the mice treated with both MG624 and taxotere took an additional 2 weeks to develop palpable tumors, another mouse

developed a palpable tumor after 18 weeks, and the remaining mouse had yet to succumb to a tumor even after 22 weeks of follow up. These results indicate that the combination of MG624 and taxotere can not only shrink a tumor to an unmeasurable volume, but this treatment also significantly delays breast cancer relapse ($p= 0.01$) in NOD/SCID mice.

To determine the mechanism whereby tumor growth was affected by MG624, taxotere, or MG624 combined with taxotere, tumors were collected from 7 mice from the control cohort, 7 mice from the MG624-treated cohort, 3 mice from the taxotere-treated cohort, and 2 mice from the MG624 + taxotere-treated cohort. Some tissue was frozen to recover viable cells, and some tissue was fixed and embedded for sectioning. Figure 9 shows H&E staining from two tumors from each cohort, at 10X and 40X magnifications (100X and 400X total magnification, respectfully). MG624 did not appear to greatly affect tumor cell morphology. If breast TICs are a rare population of cells within these tumors, we would not expect to see great effects on the majority of the cells. Treatment with taxotere led to extensive necrotic tissue in the centre of the tumors, and also had an effect on cell morphology, as many cells appear to be enlarged, with a greater cytoplasmic-to-nuclear volume than control cells, and many showed signs of apoptotic nuclei.

The combination of MG624 and taxotere led to very unique cell morphology, as the majority of one tumor section was found to have extremely large cells with fragmented nuclei, or no nuclei. Many cells appeared to be apoptotic, and others appeared to be dead or dying. In the second combination-treated tumor section, similar enlarged, apoptotic cells are also seen around the perimeter of the tumor, however this tumor

appeared slightly different in that islands of tumor cells can be seen, with few stromal cells and collagen visible throughout the tumor tissue, especially compared to taxotere-treated tumors. Similar to the taxotere-treated tumors, a large portion of the combination-treated tumors were necrotic, and very little cellular tissue could be recovered.

IF and IHC of tumor sections to elucidate the mechanism of action of MG624

TUNEL assay to quantify fragmented nuclei in spheres and tumors

In general, there are 2 types of cell death: apoptosis and necrosis. Apoptosis (also known as programmed cell death) was originally used to describe specific morphological alterations, including cytoplasmic blebbing, chromatin condensation, cell shrinkage, organelle relocalization and compaction, nuclear fragmentation, cell rounding (loss of adhesion), cell shrinkage, and the production of 'apoptotic bodies' (Bold *et al.*, 1997; Kiechle & Zhang, 2002). By contrast, necrosis is a much faster process, and does not consist of any specific cellular morphological changes. Apoptosis involves numerous biochemical pathways triggered by various cell death-inducing stimuli (Kiechle & Zhang, 2002). The TUNEL assay was developed to detect apoptotic cells via their free 3'-OH DNA ends (known as 'nicks') generated through DNA fragmentation; one of the earliest steps involved in apoptosis (Otsuki *et al.*, 2003). These DNA nicks are identified by terminal deoxynucleotidyl transferase (TdT), which catalyzes the addition of biotin-labeled dUTPs to the exposed 3' end of the fragmented DNA. Strepavidin-FITC is then used to bind to biotin, and the resultant fluorescence can be observed via fluorescence microscopy (Didenko, 2002).

Theoretically, if MG624 functions by inducing apoptosis of tumor cells, we should see an increase in apoptotic cells in tumorspheres exposed to the compound. Therefore, HCC1954 and X81 PDX sphere blocks were generated using spheres treated with 10µM of MG624 or DMSO for 48 hours. For X81 spheres, two doses of MG624 were used: 5µM and 10µM.

Apoptotic cells were detected in HCC1954 sphere block sections using the TUNEL assay (Figure 10A), which revealed that MG624-treated spheres showed an increase in the percentage of TUNEL-positive nuclei compared to DMSO-treated spheres. Interestingly, H & E staining also revealed a change in sphere morphology (Figure 10B) after 48 hours of treatment with MG624. Whereas control sphere cells contained elongated, tightly packed cells, MG624-treated spheres contained cells that were more spherical, with many dark stained nuclei (characteristic of apoptotic cells). Five spheres from both the MG624-treated and the DMSO-treated sphere blocks stained with TUNEL were chosen at random using DAPI staining, and TUNEL-positive nuclei were counted and compared to the total number of nuclei in each individual sphere. The percentage of TUNEL-positive nuclei was thus determined (Figure 10C). Treatment of HCC1954 spheres with 10µM MG624 for 48 hours was found to significantly increase the percentage of TUNEL-positive nuclei compared to vehicle-treated spheres (p-value= 1.48×10^{-6}). Therefore, MG624 induced apoptosis in the sphere-resident breast cancer cells. Figure 10D shows H & E staining of X81 spheres treated for 48 hours with MG624. These spheres were more sensitive than HCC1954 spheres, as treatment with 5µM MG624 caused spheres to dissociate and cells to show signs of fragmented nuclei and

enlarged, abnormal morphologies. At 10μM, MG624 eliminated X81 cell nuclei in the spheres, and any cells containing nuclei were swollen, with condensed chromosomes (characteristic of apoptosis). Sections were not TUNEL-stained, as MG624-treatment eliminated spheres at these concentrations.

Next, we wished to determine whether the increase in TUNEL-positive cells would translate to the tumor sections from the *in vivo* experiment. To this end, two tumors per treatment cohort (control, MG624, taxotere, and MG624 + taxotere; Figure 11) were stained with TUNEL. All tumors were found to show some degree of positive TUNEL staining. Apoptosis is a natural event that takes place during transformation, metastasis, and even repair, driving tumor progression; assuming cellular proliferation outweighs cell death (Bold *et al.*, 1997). Similar to histological findings, control and MG624-treated tumor sections comprised a similar percentage of apoptotic cells. Figure 11B shows the mean percent-TUNEL-positive nuclei for each cohort, averaged across two tumors (4 fields of view per tumor). The total nuclei counted for each cohort was as follows: 1461 nuclei in control tumors, 1494 in MG624-treated tumors, 1176 in taxotere-treated tumors, and 635 in MG624 combined with taxotere-treated tumors.

Interestingly, taxotere-treated sections displayed fewer TUNEL-positive cells (6.16% ±4.15% compared to 9.44% ±3.50%; not significant), indicating fewer cells were apoptotic in this cohort. Taxotere is known to interfere with cell division, and induce apoptosis in mitotic cells (Bold *et al.*, 1997). Therefore the decrease in apoptotic cells observed in the taxotere-treated cohort is intriguing, and may be a sign of chemotherapy-resistance in these tumors. Most importantly, MG624 significantly increased the

percentage of apoptotic cells when combined with chemotherapy, compared to controls and chemotherapy alone (p-value= 0.0015), establishing one mechanism by which MG624 in combination with chemotherapy functions to shrink tumors *in vivo*.

Ki-67 IHC to assess tumor cell proliferation

Ki-67 is a nuclear protein that is often used as a marker of proliferation, as it is not expressed in quiescent cells (Gerdes *et al.,* 1984), and is universally expressed in proliferating cells. Ki67 is frequently used in the clinic as an indicator of patient tumor proliferation, and has been found to be consistent and reproducible (Urruticoechea *et al.*, 2005). Therefore, IHC was performed on tumor sections from the *in vivo* experiment to assess differences in Ki-67 expression among the tumors from the 4 treatment cohorts. Two tumors from each cohort were used to quantify the average percentage of Ki-67 positive cells from three fields of view (Figure 12A). Obvious differences can be observed between treatment groups with regards to staining intensity, however, once all Ki-67 positive cells were quantified, it was discovered that there were no statistically significant differences among the treatment groups for percent Ki-67 positivity (Figure 12B).

However, Ki-67 is not expressed equally throughout the cell cycle. In G1, it is expressed very weakly, and stains weak foci in the karyoplasm. In late G1, it condenses in larger perinucleolar granules. By G2/S phase, Ki-67 is primarily localized to the nucleolus, and the staining intensity increases (compared to G1). In early M-phase (mitosis), when the nuclear membrane disrupts, Ki-67 expression becomes very intense, as it is now being expressed in the cytoplasm on the surface of condensed chromosomes.

By anophase-telophase, this intensity begins to dissipate (Starborg *et al.*, 1996). Consequently, Ki-67 staining is not able to differentiate cells arrested in G1, G2, or S from those actively proliferating. Therefore, based on staining intensity and localization, Ki-67-positive cells were re-quantified, separating cells into G1, G2/S, and M-phase (Figure 12C). The relative proportions of cells in the different phases of the cell cycle revealed that the majority of Ki-67-positive cells are in G1, while only a fraction of cells are in G2/S or M. Similar proportions of cells in each treatment group were found to be in G2, however differences could be seen in cells currently in the M-phase of the cell cycle; the combination of MG624 and taxotere nearly eliminated cells in this phase. Therefore, additional analyses were performed in order to determine if these differences were significant (Figure 12D). This analysis revealed that the combination of MG624 and taxotere significantly reduced the percentage of cells undergoing mitosis in comparison to controls and taxotere treatment alone (p-value= 0.0009). Interestingly, MG624 alone also showed a marked decrease in M-phase cells (n/s). This could indicate that the combination of MG624 and taxotere arrests cells in G2, which could be the mechanism whereby MG624 and taxotere induce apoptosis, or it could be another mechanism whereby MG624 and taxotere treatment leads to the decrease in tumor volume.

IF staining to assess markers of differentiation: CK8 and α-SMA

An additional mechanism to target BTICs would be to force them into a differentiation program, as they would not only lose their ability to self-renew, but their proliferative capacity would be reduced and they may be more sensitive to chemotherapy. Therefore, treated tumor sections were stained with CK8 (a luminal cytokeratin marker)

and α-SMA (a myoepithelial cell marker) to assess whether any treatment enriched for cells of a specific lineage (Figure 13A). Control tumors, while made up of mostly $CK8^+$ cells, were found to contain cells that expressed both luminal and myoepithelial markers, possibly indicating that these cells are progenitor-like cells. MG624-treated tumor sections, on the other hand, seemed to express both markers equally, however never on the same cell, possibly indicating that there are fewer progenitor cells in these tumors, however the difference between MG624-treated tumors and control tumors is not very apparent. Taxotere-treated tumors also seemed to have equal proportions of $CK8^+$ and α-SMA^+ cells, however the majority of α-SMA^+ cells were elongated and spindle-shaped, which indicates that they are either fibroblasts, or cells undergoing EMT. Interestingly, the tumor sections from the MG624 combined with taxotere-treated cohort stained entirely negative for α-SMA within tumor tissue. Therefore the combination treatment of MG624 and taxotere enriched for $CK8^+$ cells (Figure 13A).

In order to determine whether α-SMA staining from Figure 13A is detecting human myoepithelial cells or mouse fibroblasts, human mitochondrial (HuMt) antibodies were also used to stain these tumor sections (Figure 13B). In the control and MG624 treated sections, there was a significant overlap between α-SMA^+ and $HuMt^+$ cells, indicating that these cells are indeed human myoepithelial cells. The taxotere-treated section, on the other hand, did not have any overlapping cell staining, indicating that these α-SMA^+ cells are not human. Based on their spindle-shape, it is likely that they are mouse fibroblasts that have been recruited to the tumor. Therefore taxotere alone enriched for $CK8^+$ cells. In the MG624 combined with taxotere-treated cohort, there are no α-

SMA^+ cells, only $CK8^+$ cells, indicating that while taxotere appeared to recruit fibroblasts to the tumor, MG624 in combination with taxotere eliminated fibroblasts. This is quite interesting, as this could be another method whereby MG624 functions to shrink tumors *in vivo*.

CHAPTER 4: DISCUSSION

The high rate of recurrence following conventional therapies in breast cancer patients has been attributed to a small subset of drug-resistant cells that are ultimately responsible for reseeding a new tumor post-therapy. With the vast advancements made in the field of breast cancer research, relapse remains a major burden on both patients and the health care system, demonstrating a great need for the discovery of novel therapies or combinations of therapies that can target TICs, as well as their non-tumorigenic descendants (Ponti *et al.*, 2005; Ma *et al.*, 2013). Here we have shown that nAChR antagonists can be used to specifically target breast CSCs, and are therefore of particular interest for future breast cancer treatments. In particular, we have shown that MG624, an α7 and α4β2 nAChR antagonist, displays a uniquely high specificity for sphere-forming cells, as its effects on sphere formation cannot be fully appreciated until the compound is removed, and secondary spheres are seeded. This is an excellent demonstration that MG624 interferes with the self-renewal of sphere-forming cells, and that the non-tumorigenic bulk of the cells in these spheres were only affected by increasing doses of MG624, as demonstrated by post-treatment colony forming assays, where colonies grew at MG624 pre-treatment doses that were found to completely inhibit sphere formation. A

likely hypothesis for these observations is that MG624 targets breast cancer cells in a hierarchal manner, starting with the sphere-forming cell having the greatest sensitivity towards MG624, followed by cells capable of adherent proliferation (colony formation), and lastly, cells that make up the remaining bulk of a sphere, which do not have proliferative capabilities, but are viable. This hierarchal nature of MG624 specificity is quite unique. These data were also confirmed using multiple breast cancer cell lines, as well as PDX spheres, which are a closer representation to patient tumors than immortalized cell lines.

Congruently, when combined with chemotherapy (taxotere or doxorubicin), MG624 was found to be a chemosynergizer, meaning that lower doses of both MG624 and chemotherapy could be used and produce a greater effect than either drug alone. Due to the toxic effects of increasing doses of chemotherapy for patients (Azim *et al.*, 2011), this is very promising. Furthermore, MG624 was found to target functional BTICs in *ex vivo* assays, which is an important validation of the unique *in vitro* data.

Importantly, MG624 could be combined with taxotere chemotherapy in order to shrink tumors, and delay/prevent relapse in HCC1954-derived tumor bearing NOD/SCID mice that had been 'cured' of palpable tumors after 3 weeks of treatment. This combination therapy was further analyzed, and it was determined that tumors were shrinking due to a decrease in cells entering the M-phase of the cell cycle, perhaps through G1 or G2 cell cycle arrest. nAChR signaling primarily involves the influx of cations, and in particular, Ca^{2+}, which is known to be required for cell-cycle progression, specifically the progression of cells through the G1 phase of the cell cycle into the S-

phase (Prevarskaya *et al.*, 2010). Inhibiting this pathway would therefore interfere with cell cycle progression. This hypothesis could be confirmed in future studies by staining for cell cycle regulator proteins, such as cyclin-dependent kinase inhibitor 1 (p21) or inactivated M-phase inducer phosphatase 3 (p-Cdc25C) (Wu *et al.*, 2002; Yan *et al.*, 2005). Similarly, taxotere interferes with mitosis during the cell cycle by obstructing the lengthening and shortening of microtubules in a cell, causing abnormal microtubule assembly and preventing cells from transitioning from metaphase to anaphase. Therefore when MG624 and taxotere were combined, it makes sense that so few cells enter into the M-phase, as demonstrated by Ki-67 staining.

Cell cycle arrest in G2/M phase can lead to temporary or permanent cell senescence, or could be involved in inducing cell apoptosis. We have shown that MG624 in combination with taxotere increases the percentage of TUNEL-positive nuclei, confirming that this combination does indeed lead to induction of apoptosis. Therefore our data suggests that the combination of MG624 and taxotere leads to the induction of breast cancer cell apoptosis through cell cycle arrest. Taxotere interferes with microtubule disassembly, leading to an accumulation of microtubules, and induction of apoptosis (Yvon *et al.*, 1999). Taxotere has also been found to play a role in the Bcl-2/BAX pathway, another mechanism of apoptosis induction (Moos & Fitzpatrick, 1998). Therefore, it could be expected that taxotere would induce apoptosis *in vivo*, which would be evident in our tumor sections. Interestingly, the reverse was observed: taxotere-treated sections displayed less apoptotic cells compared to the control. This could indicate that the ‘snapshot’ we took of the effect of taxotere on tumors missed the majority of the

apoptosis (or necrosis) that would have taken place, resulting in the cease of tumor growth that was observed. The tumor tissue that was able to be collected was also very minimal in comparison to control tumors, and H & E staining revealed a large section of necrosis in these tumors—evidence of destruction that took place during treatment, before tumors were harvested. Therefore, it could be speculated that the difference in TUNEL-positive nuclei observed between control tumors and taxotere-treated tumors is not relevant, as long as cells are not proliferating faster than other cells are dying, tumors should still shrink with taxotere-treatment alone. However, Ki-67 staining revealed that cells are still proliferating at a similar rate to control tumors, and more importantly, the percentage of cells in the M-phase of the cell cycle are on par with control tumor sections. Whether or not these cells are arrested mid-M-phase cannot be determined, however, if that was the case, we would expect to see this reflected in the TUNEL staining, as cells arrested in the M-phase would inevitably induce apoptosis due to the accumulation of microtubules (Yvon *et al.*, 1999). Therefore, it could be argued that the taxotere tumor sections may be displaying properties of chemo-resistance, which is a common occurrence in patients treated with chemotherapy (Honma *et al.*, 2008).

If MG624 is responsible for targeting chemo-resistant BTICs in tumors, this would explain why the combination of treatments effectively shrunk tumors and even cured the majority of the mice. Alone, MG624 may target BTICs within a tumor, but has a very low selectivity for the non-tumorigenic bulk of the tumor, explaining why combining it with chemotherapy would be effective. Taxotere was able to target the majority of the cells in the tumor, and MG624 was able to target the chemo-resistant

BTICs. This is further supported by the finding that alone, taxotere successfully inhibited the growth of tumors, but was never able to cure any mice until it was combined with MG624.

One very interesting finding that was observed was taxotere-treated tumor sections stained high for α-SMA, but none of the positive cells were of human origin. On the other hand when combined with MG624, intratumoral α-SMA-positive cells were completely eliminated, leading to the enrichment of $CK8^+$ cells. The non-human α-SMA-positive cells were determined to be mouse fibroblasts, as they can be identified in tumor tissue based on their spindle shape, and high expression of α-SMA (Yamashita *et al.*, 2012; Fang *et al.*, 2014). CAFs have been found to play an important role in epithelial tumor biology. In particular, the myofibroblast (a key cell involved in wound healing via connective tissue remodeling) plays an important role in tumor invasion and metastasis (De Wever & Mareel, 2003). The appearance of fibroblasts and myofibroblasts expressing α-SMA, and the associated stromal changes, is known as the "desmoplastic reaction" (Yamashita *et al.*, 2012). High α-SMA expression (due to the presence of myofibroblasts), compared to low α-SMA expression, has been correlated to a significantly poorer overall survival rate in breast cancer patients, as well as a shorter time-to-metastasis (Yamashita *et al.*, 2012).

The presence of intratumoral fibroblasts has been found to lead to a dramatic decrease in chemotherapeutic drug uptake, possibly through the production of collagen type I, leading to an increased interstitial fluid pressure (Heldin *et al.*, 2004). In fact, targeting fibroblasts in the tumor stroma has been found to lead to greater than 70%

improvement in tumor cell drug uptake (Loeffler *et al.*, 2006). Furthermore, fibroblasts are involved in angiogenesis and tumor growth (Orimo *et al.*, 2005).

FGFR signaling has been found to be crucial for stem cell self-renewal, and interfering with FGFR signaling has been found to lead to cell differentiation in dental epithelial stem cells (DESCs) (Chang *et al.*, 2013). The presence of stromal fibroblasts has been found to increase the proliferation of the $CD44^{+}/CD24^{-}$ population of mammospheres (Huang *et al.*, 2010), and FGFR signalling has also been found to promote triple negative breast cancer cell growth (Sharpe *et al.*, 2012). Interestingly, stimulation of nAChRs by epibatidine, a potent nAChR agonist, has been found to increase mRNA and protein levels of FGF-2 in the brain, indicating that FGF-2 may be a downstream transcriptional target involved in nAChR signalling (Belluardo *et al.*, 1999). It was also found that MG624 binding to nAChRs leads to a decrease in FGF-2 mRNA expression levels as well (Brown *et al.*, 2012).

Therefore, MG624 may be interfering with FGF-2 signalling, potentially through BTICs within the tumor tissue. This in effect would prevent the taxotere-induced recruitment of CAFs into the tumor, thereby allowing taxotere full access to the tumor tissue, preventing tumor chemo resistance. nAChR signalling is complicated, and numerous proliferative cellular pathways have been implicated in nAChRs and cancer development (Ambrosi & Becchetti, 2013). Therefore the effect of MG624 on breast cancer cells may function through multiple downstream pathways, and down regulation of FGF-2 may be just one of many pathways down regulated, presenting only *in vivo*.

It is possible, however, that the effect of MG624 *in vitro* may be unrelated to the *in vivo* effect that is being seen. MG624 could be inducing cell senescence, which would explain why the effect of the compound is more apparent in a secondary sphere-forming assay, why MG624 synergized with chemotherapy, and why tumor development was delayed in *ex vivo* experiments. Therefore the *in vitro* effects could potentially be an artifact, and the effect seen *in vivo* could actually be due to MG624 eliminating intratumoral fibroblasts, allowing chemotherapy access to the entirety of the tumor tissue. Therefore, in order to confirm that MG624 in combination with taxotere is indeed targeting functional BTICs, limiting dilution cell transplants of tumor tissue collected after treatment with MG624 in combination with taxotere would have to be injected into naïve mice. Unfortunately, there was not enough tumor tissue from any of the mice in our combination-treated cohort to warrant such an experiment. Thus future experiments should include treating a larger cohort of mice, and sacrificing them earlier in order to harvest tumors large enough for serial transplants. Additionally, another important future experiment should involve different nAChR subunits being knocked down using siRNA in breast cancer cells in order to determine which nAChR subunits MG624 is actually binding to in order to exert its effects. Unfortunately, due to the lack of available binding studies in the literature, our pharmaceutical data was unable to conclusively identify the important nAChR responsible for BTIC self-renewal and proliferation.

CONCLUSION

These results demonstrate than nAChRs may be important for the self-renewal and survival of BTICs. MG624, an α7 and α4β2 nAChR antagonist, was shown to specifically target sphere-forming cells *in vitro*, synergize with chemotherapy in breast cancer cells grown as spheres *in vitro*, specifically target functional TICs in an *ex vivo* assay, and in combination with taxotere, shrink tumors and prevent tumor progression/relapse *in vivo* in immunodeficient mice bearing HCC1954 human breast cancer cell line-derived mammary tumors. The combination of MG624 and taxotere was found to induce apoptosis in tumors after 3 weeks of treatment, and in established spheres after 48 hours of treatment. The combination of MG624 and taxotere was also found to potentially arrest cells in G2, preventing cells from entering mitosis. Finally, MG624 in combination with taxotere was found to eliminate fibroblasts, possibly through the down regulation of FGF-2 transcription, thereby enriching for $CK8^+$ cells, which has been found to have a better prognosis for breast cancer patients. Therefore MG624 functions as a highly specific, efficacious BTIC inhibitor, and when combined with chemotherapy, may be a promising treatment for breast cancer patients.

REFERENCES

Allison, K.H. (2012). Molecular pathology of breast cancer: what a pathologist needs to know. *Am. J. Clin. Pathol.* **138**, 770–80.

Ambrosi, P. & Becchetti, A. (2013). Targeting Neuronal Nicotinic Receptors in Cancer: New Ligands and Potential Side-Effects. *Recent Pat. Anticancer. Drug Discov.* **8**, 38–52.

Amici, S., McKay, S., Wells, G., Robson, J., Nasir, M., Ponath, G., *et al.* (2012). A highly conserved cytoplasmic cysteine residue in the α4 nicotinic acetylcholine receptor is palmitoylated and regulates protein expression. *J. Biol. Chem.* **287**, 23119–27.

Aracava, Y., Pereira, E.F.R., Maelicke, A. & Albuquerque, E.X. (2005). Memantine blocks alpha7 nicotinic acetylcholine receptors more potently than N-methyl- D - aspartate receptors in rat hippocampal neurons **312**, 1195–1205.

Azim, H., de Azambuja, E., Colozza, M., Bines, J. & Piccart, M.J. (2011). Long-term toxic effects of adjuvant chemotherapy in breast cancer. *Ann. Oncol.* **22**, 1939–47.

Baccelli, I. & Trumpp, A. (2012). The evolving concept of cancer and metastasis stem cells. *J. Cell Biol.* **198**, 281–93.

Battershill, J.M. (2005). The Multiple Chemicals and Actions model of carcinogenesis. A possible new approach to developing prevention strategies for environmental carcinogenesis. *Hum. Exp. Toxicol.* **24**, 547–58.

Belluardo, N., Mudò, G., Blum, M., Cheng, Q., Caniglia, G., Dell'Albani, P., *et al.* (1999). The nicotinic acetylcholine receptor agonist (+/-)-epibatidine increases FGF-2 mRNA and protein levels in the rat brain. *Brain Res. Mol. Brain Res.* **74**, 98–110.

Bertrand, D., Ballivet, M. & Rungger, D. (1990). Activation and blocking of neuronal nicotinic acetylcholine receptor reconstituted in Xenopus oocytes. *Proc. Natl. Acad. Sci. U. S. A.* **87**, 1993–7.

Bold, R.J., Termuhlen, P.M. & McConkey, D.J. (1997). Apoptosis, cancer and cancer therapy. *Surg. Oncol.* **6**, 133–42.

Brown, D. a. (2006). Acetylcholine. *Br. J. Pharmacol.* **147 Suppl** , S120–6.

Brown, K.C., Lau, J.K., Dom, A.M., Witte, T.R., Luo, H., Crabtree, C.M., *et al.* (2012). MG624, an α7-nAChR antagonist, inhibits angiogenesis via the Egr-1/FGF2 pathway. *Angiogenesis* **15**, 99–114.

Buisson, B. & Bertrand, D. (1998). Open-channel blockers at the human alpha4/beta2 neuronal nicotinic acetylcholine receptor. *Mol. Pharmacol.* **563**, 555–563.

Chang, J.Y.F., Wang, C., Liu, J., Huang, Y., Jin, C., Yang, C., *et al.* (2013). Fibroblast growth factor signaling is essential for self-renewal of dental epithelial stem cells. *J. Biol. Chem.* **288**, 28952–61.

Changeux, J.-P. (2010). Nicotine addiction and nicotinic receptors: lessons from genetically modified mice. *Nat. Rev. Neurosci.* **11**, 389–401.

Chavez-noriega, L.E., Crona, J.H., Washburn, M.S., Urrutia, A., Elliott, K.J. & Johnson, E.C. (1997). Pharmacological characterization of recombinant human neuronal nicotinic acetylcholine receptors ha2b2, ha2b4, ha3b2, hab4, ha4b2, ha4b4, ha7 expressed in xenopus oocytes. *J. Pharmacol. Exp. Ther.* **280**, 346–356.

Chédotal, a, Kerjan, G. & Moreau-Fauvarque, C. (2005). The brain within the tumor: new roles for axon guidance molecules in cancers. *Cell Death Differ.* **12**, 1044–56.

Chen, H.-S.V. & Lipton, S. a. (2006). The chemical biology of clinically tolerated NMDA receptor antagonists. *J. Neurochem.* **97**, 1611–26.

Corringer, P.-J., Poitevin, F., Prevost, M.S., Sauguet, L., Delarue, M. & Changeux, J.-P. (2012). Structure and pharmacology of pentameric receptor channels: from bacteria to brain. *Structure* **20**, 941–56.

Creighton, C.J., Li, X., Landis, M., Dixon, J.M., Neumeister, V.M., Sjolund, A., *et al.* (2009). Residual breast cancers after conventional therapy display mesenchymal as well as tumor-initiating features. *Proc. Natl. Acad. Sci. U. S. A.* **106**, 13820–5.

D'hoedt, D. & Bertrand, D. (2009). Nicotinic acetylcholine receptors: an overview on drug discovery. *Expert Opin. Ther. Targets* **13**, 395–411.

Dale, H.H. & Dudley, H.W. (1929). The presence of histamine and acetylcholine in the spleen of the ox and the horse. *J. Physiol.* **68**, 97–123.

Dasgupta, P., Kinkade, R., Joshi, B., Decook, C., Haura, E. & Chellappan, S. (2006). Nicotine inhibits apoptosis induced by chemotherapeutic drugs by up-regulating XIAP and survivin. *Proc. Natl. Acad. Sci. U. S. A.* **103**, 6332–7.

Dean, M., Fojo, T. & Bates, S. (2005). Tumour stem cells and drug resistance. *Nat. Rev. Cancer* **5**, 275–84.

Diamandis, P., Wildenhain, J., Clarke, I.D., Sacher, A.G., Graham, J., Bellows, D.S., *et al.* (2007). Chemical genetics reveals a complex functional ground state of neural stem cells. *Nat. Chem. Biol.* **3**, 268–73.

Didenko, V. V. (2002). TUNEL assay: An overview of techniques. In *In Situ Detection of DNA Damage: Methods and Protocols*: 21–31.

Dollé, L., El Yazidi-Belkoura, I., Adriaenssens, E., Nurcombe, V. & Hondermarck, H. (2003). Nerve growth factor overexpression and autocrine loop in breast cancer cells. *Oncogene* **22**, 5592–601.

Dontu, G., Abdallah, W.M., Foley, J.M., Jackson, K.W., Clarke, M.F., Kawamura, M.J., *et al.* (2003). In vitro propagation and transcriptional profiling of human mammary stem / progenitor cells. *Genes Dev.* **17**, 1253–1270.

Egleton, R.D., Brown, K.C. & Dasgupta, P. (2008). Nicotinic acetylcholine receptors in cancer: multiple roles in proliferation and inhibition of apoptosis. *Trends Pharmacol. Sci.* **29**, 151–8.

Elgoyhen, a B., Vetter, D.E., Katz, E., Rothlin, C. V, Heinemann, S.F. & Boulter, J. (2001). Alpha10: a determinant of nicotinic cholinergic receptor function in mammalian vestibular and cochlear mechanosensory hair cells. *Proc. Natl. Acad. Sci. U. S. A.* **98**, 3501–6.

Entschladen, F., Palm, D., Niggemann, B. & Zaenker, K.S. (2008). The cancer's nervous tooth: Considering the neuronal crosstalk within tumors. *Semin. Cancer Biol.* **18**, 171–5.

Evans, K.K., Birdwell, R.L. & Wolfe, J.M. (2013). If you don't find it often, you often don't find it: why some cancers are missed in breast cancer screening. *PLoS One* **8**, e64366.

Falsafi, S.K., Deli, A., Höger, H., Pollak, A. & Lubec, G. (2012). Scopolamine administration modulates muscarinic, nicotinic and NMDA receptor systems. *PLoS One* **7**, e32082.

Fang, W. Bin, Yao, M. & Cheng, N. (2014). Priming cancer cells for drug resistance: role of the fibroblast niche. *Front. Biol. (Beijing).* **9**, 114–126.

Fedorov, N.B., Benson, L.C., Graef, J. & Lippiello, P.M. (2009). Differential pharmacologies of mecamylamine enantiomers : Positive allosteric modulation and noncompetitive inhibition **328**, 525–532.

Ferlay, J., Soerjomataram, I., Ervik, M., Dikshit, R., Eser, S., Mathers, C., *et al.* (2013). Cancer Incidence and Mortality Worldwide: IARC CancerBase No. 11. GLOBOCAN 2012 v1.0. *Lyon, Fr. Int. Agency Res. Cancer* http://globocan.iarc.fr.

Fillmore, C.M. & Kuperwasser, C. (2008). Human breast cancer cell lines contain stem-like cells that self-renew, give rise to phenotypically diverse progeny and survive chemotherapy. *Breast Cancer Res.* **10**, R25.

Geldof, A.A., Van Haarst, E.P. & Newling, D.W.W. (1998). Neurotrophic factors in prostate and prostatic cancer. *Prostate Cancer Prostatic Dis.* **1**, 236–241.

Gentry, C.L. & Lukas, R.J. (2001). Local anesthetics noncompetitively inhibit function of four distinct nicotinic acetylcholine receptor subtypes. *J. Pharmacol. Exp. Ther.* **299**, 1038–48.

Gerdes, J., Lemke, H., Baisch, H., Wacker, H.H., Schwab, U. & Stein, H. (1984). Cell cycle analysis of a cell proliferation-associated human nuclear antigen defined by the monoclonal antibody Ki-67. *J. Immunol.* **133**, 1710–5.

Goodell, M.A., Brose, K., Paradis, G., Conner, A.S. & Mulligan, R.C. (1996). Isolation and Functional Properties of Murine Hematopoietic Stem Cells that are Replicating In Vivo. *J. Exp. Med.* **183**, 1797–1806.

Gotti, C., Balestra, B., Moretti, M., Rovati, G.E., Maggi, L., Rossoni, G., *et al.* (1998). 4-Oxystilbene compounds are selective ligands for neuronal nicotinic alphaBungarotoxin receptors. *Br. J. Pharmacol.* **124**, 1197–206.

Gotti, C. & Clementi, F. (2004). Neuronal nicotinic receptors: from structure to pathology. *Prog. Neurobiol.* **74**, 363–96.

Grabowski, P., Schindler, I., Anagnostopoulos, I., Foss, H.D., Riecken, E.O., Mansmann, U., *et al.* (2001). Neuroendocrine differentiation is a relevant prognostic factor in stage III-IV colorectal cancer. *Eur. J. Gastroenterol. Hepatol.* **13**, 405–11.

Granda, T.G., Filipski, E., Attino, R.M.D. & et. al. (2001). Experimental chronotherapy of mouse mammary adenocarcinoma MA13/C with docetaxel and doxorubicin as single agents and in combination. *Cancer Res.* **61**, 1996–2001.

Grimshaw, M.J., Cooper, L., Papazisis, K., Coleman, J. a, Bohnenkamp, H.R., Chiapero-Stanke, L., *et al.* (2008). Mammosphere culture of metastatic breast cancer cells enriches for tumorigenic breast cancer cells. *Breast Cancer Res.* **10**, R52.

Guy, J.J. & Hamor, T.A. (1973). Crystal and molecular structure of adiphenine hydrochloride, a muscarinic antagonist of acetylcholine. *J. Chem. Soc. Perkin Trans. 2* 942–947.

Hallett, R.M. (2012). *Using gene expression analysis to guide and identify treatments for breast cancer patients.* Ph.D. Thesis. McMaster University, Canada.

Hanahan, D. & Weinberg, R. (2011). Hallmarks of cancer: the next generation. *Cell* **144**, 646–74.

Hassane, D.C., Guzman, M.L., Corbett, C., Li, X., Abboud, R., Young, F., *et al.* (2008). Discovery of agents that eradicate leukemia stem cells using an in silico screen of public gene expression data. *Blood* **111**, 5654–5662.

Hecht, S.S. (2012). Research opportunities related to establishing standards for tobacco products under the Family Smoking Prevention and Tobacco Control Act. *Nicotine Tob. Res.* **14**, 18–28.

Heeschen, C., Jang, J.J., Weis, M., Pathak, a, Kaji, S., Hu, R.S., *et al.* (2001). Nicotine stimulates angiogenesis and promotes tumor growth and atherosclerosis. *Nat. Med.* **7**, 833–9.

Heldin, C.-H., Rubin, K., Pietras, K. & Ostman, A. (2004). High interstitial fluid pressure - an obstacle in cancer therapy. *Nat. Rev. Cancer* **4**, 806–13.

Hillmer, A.T., Wooten, D.W., Farhoud, M., Barnhart, T.E., Mukherjee, J. & Christian, B.T. (2013). The effects of lobeline on α4β2 nicotinic acetylcholine receptor binding and uptake of [(18)F]nifene in rats. *J. Neurosci. Methods* **214**, 163–169.

Hirata, N., Sekino, Y. & Kanda, Y. (2010). Nicotine increases cancer stem cell population in MCF-7 cells. *Biochem. Biophys. Res. Commun.* **403**, 138–43.

Honma, K., Iwao-Koizumi, K., Takeshita, F., Yamamoto, Y., Yoshida, T., Nishio, K., *et al.* (2008). RPN2 gene confers docetaxel resistance in breast cancer. *Nat. Med.* **14**, 939–48.

Hotchkiss, K.A., Ashton, A.W., Mahmood, R., Russell, R.G., Sparano, J.A. & Schwartz, E.L. (2002). Inhibition of endothelial cell function in vitro and angiogenesis in vivo by docetaxel (taxotere): Association with impaired repositioning of the microtubule organizing center. *Mol. Cancer Ther.* **1**, 1191–1200.

Hu, Z., Fan, C., Oh, D.S., Marron, J.S., He, X., Qaqish, B.F., *et al.* (2006). The molecular portraits of breast tumors are conserved across microarray platforms. *BMC Genomics* **7**, 96.

Huang, M., Li, Y., Zhang, H. & Nan, F. (2010). Breast cancer stromal fibroblasts promote the generation of CD44+CD24- cells through SDF-1/CXCR4 interaction. *J. Exp. Clin. Cancer Res.* **29**, 80.

Jiang, Z.W., Gong, Q.Z., Di, X., Zhu, J. & Lyeth, B.G. (2000). Dicyclomine, an M1 muscarinic antagonist, reduces infarct volume in a rat subdural hematoma model. *Brain Res.* **852**, 37–44.

Johnson, D.S., Michael, J. & Heinemann, F. (1995). Alpha-conotoxin imi exhibits subtype-specific nicotinic acetylcholine receptor blockade : Preferential inhibition of homomeric a7 and a9 receptors. *Mol. Pharmacol.* **48**, 194–199.

Kiechle, F.L. & Zhang, X. (2002). Apoptosis: biochemical aspects and clinical implications. *Clin. Chim. Acta.* **326**, 27–45.

Kondratyev, M., Kreso, a, Hallett, R.M., Girgis-Gabardo, a, Barcelon, M.E., Ilieva, D., *et al.* (2012). Gamma-secretase inhibitors target tumor-initiating cells in a mouse model of ERBB2 breast cancer. *Oncogene* **31**, 93–103.

Korkaya, H., Kim, G.-I., Davis, A., Malik, F., Henry, N.L., Ithimakin, S., *et al.* (2012). Activation of an IL6 inflammatory loop mediates trastuzumab resistance in HER2+ breast cancer by expanding the cancer stem cell population. *Mol. Cell* **47**, 570–84.

Kurpios, N. a, MacNeil, L., Shepherd, T.G., Gludish, D.W., Giacomelli, A.O. & Hassell, J. a. (2009). The Pea3 Ets transcription factor regulates differentiation of multipotent progenitor cells during mammary gland development. *Dev. Biol.* **325**, 106–21.

Kurpios, N., Girgis-Gabardo, A., Hallett, R.M., Rogers, S., Gludish, D.W., Kockeritz, L., *et al.* (2013). Single unpurified breast tumor-initiating cells from multiple mouse models efficiently elicit tumors in immune-competent hosts. *PLoS One* **8**, e58151.

Lamb, J., Crawford, E.D., Peck, D., Modell, J.W., Blat, I.C., Wrobel, M.J., *et al.* (2006). The Connectivity Map: using gene-expression signatures to connect small molecules, genes, and disease. *Science* **313**, 1929–35.

Lee, C.-H., Huang, C.-S., Chen, C.-S., Tu, S.-H., Wang, Y.-J., Chang, Y.-J., *et al.* (2010). Overexpression and activation of the alpha9-nicotinic receptor during tumorigenesis in human breast epithelial cells. *J. Natl. Cancer Inst.* **102**, 1322–35.

Lenzken, S.C., Lanni, C., Govoni, S., Lucchelli, A., Schettini, G. & Racchi, M. (2007). Nicotinic component of galantamine in the regulation of amyloid precursor protein processing. *Chem. Biol. Interact.* **165**, 138–45.

Levina, V., Marrangoni, A., Wang, T., Parikh, S., Su, Y., Herberman, R., *et al.* (2010). Elimination of human lung cancer stem cells through targeting of the stem cell factor-c-kit autocrine signaling loop. *Cancer Res.* **70**, 338–46.

Lhommé, C., Joly, F., Walker, J.L., Lissoni, A., Nicoletto, M.O., Manikhas, G.M., *et al.* (2008). Phase III study of valspodar (PSC 833) combined with paclitaxel and carboplatin compared with paclitaxel and carboplatin alone in patients with stage IV or suboptimally debulked stage III epithelial ovarian cancer or primary peritoneal cancer. *J. Clin. Oncol.* **26**, 2674–82.

Li, X., Lewis, M.T., Huang, J., Gutierrez, C., Osborne, C.K., Wu, M.-F., *et al.* (2008). Intrinsic resistance of tumorigenic breast cancer cells to chemotherapy. *J. Natl. Cancer Inst.* **100**, 672–9.

Lin, W., Hirata, N., Sekino, Y. & Kanda, Y. (2012). Role of α7-nicotinic acetylcholine receptor in normal and cancer stem cells. *Curr. Drug Targets* **13**, 656–65.

Loeffler, M., Kruger, J.A., Niethammer, A.G. & Reisfeld, R.A. (2006). Targeting tumor-associated fibroblasts improves cancer chemotherapy by increasing intratumoral drug uptake. *J. Clin. Invest.* **116**, 1955–1962.

López-Muñoz, F. & Alamo, C. (2009). Historical evolution of the neurotransmission concept. *J. Neural Transm.* **116**, 515–33.

Lotti, F., Jarrar, A.M., Pai, R.K., Hitomi, M., Lathia, J., Mace, A., *et al.* (2013). Chemotherapy activates cancer-associated fibroblasts to maintain colorectal cancer-initiating cells by IL-17A. *J. Exp. Med.* **210**, 2851–72.

Ma, X., Zhou, J., Zhang, C.-X., Li, X.-Y., Li, N., Ju, R.-J., *et al.* (2013). Modulation of drug-resistant membrane and apoptosis proteins of breast cancer stem cells by targeting berberine liposomes. *Biomaterials* http://dx.doi.org/10.1016/j.biomaterials.2013.02.0.

Magee, J., Piskounova, E. & Morrison, S.J. (2012). Cancer stem cells: impact, heterogeneity, and uncertainty. *Cancer Cell* **21**, 283–96.

Mai, H., May, W.S., Gao, F., Jin, Z. & Deng, X. (2003). A functional role for nicotine in Bcl2 phosphorylation and suppression of apoptosis. *J. Biol. Chem.* **278**, 1886–91.

Mancino, M., Ametller, E., Gascón, P. & Almendro, V. (2011). The neuronal influence on tumor progression. *Biochim. Biophys. Acta* **1816**, 105–18.

Mansi, J.L., Yellowlees, A., Lipscombe, J., Earl, H.M., Cameron, D., Coleman, R.E., *et al.* (2010). Five-year outcome for women randomised in a phase III trial comparing

doxorubicin and cyclophosphamide with doxorubicin and docetaxel as primary medical therapy in early breast cancer: an Anglo-Celtic Cooperative Oncology Group study. *Breast Cancer Res. Treat.* **122**, 787–94.

Matsubayashi, H., Alkondon, M., Pereira, E.F., Swanson, K.L. & Albuquerque, E.X. (1998). Strychnine: a potent competitive antagonist of alpha-bungarotoxin-sensitive nicotinic acetylcholine receptors in rat hippocampal neurons. *J. Pharmacol. Exp. Ther.* **284**, 904–13.

May, C.D., Sphyris, N., Evans, K.W., Werden, S.J., Guo, W. & Mani, S. (2011). Epithelial-mesenchymal transition and cancer stem cells: a dangerously dynamic duo in breast cancer progression. *Breast Cancer Res.* **13**, 202.

Millar, N.S. (2003). Assembly and subunit diversity of nicotinic acetylcholine receptors. *Biochem. Soc. Trans.* **31**, 869–74.

Millward, M.J., Cantwell, B.M., Munro, N.C., Robinson, A., Corris, P. & Harris, L. (1993). Oral verapamil with chemotherapy for advanced non-small cell lung cancer: a randomised study. *Br. J. Cancer* **67**, 1031–5.

Misset, J.L., Dieras, V., Gruia, G., Bourgeois, H., Cvitkovic, E., Kalla, S., *et al.* (1999). Dose-finding study of docetaxel and doxorubicin in first-line treatment of patients with metastatic breast cancer. *Ann. Oncol.* **10**, 553–560.

Mitchell, B.S., Schumacher, U., Stauber, V. V & Kaiserling, E. (1994). Are breast tumours innervated? Immunohistological investigations using antibodies against the neuronal marker protein gene product 9.5 (PGP 9.5) in benign and malignant breast lesions. *Eur. J. Cancer* **30A**, 1100–3.

Mogg, A.J., Whiteaker, P., McIntosh, J.M., Marks, M., Collins, A.C. & Wonnacott, S. (2002). Methyllycaconitine is a potent antagonist of alpha-conotoxin-MII-sensitive presynaptic nicotinic acetylcholine receptors in rat striatum. *J. Pharmacol. Exp. Ther.* **302**, 197–204.

Moos, J. & Fitzpatrick, F.A. (1998). Taxanes propagate apoptosis via two cell populations with distinctive cytological and molecular traits. *Cell growth Differ.* **9**, 687–697.

Mukhin, A.G., Undisch, D.G., Horti, A.G., Koren, A.O., Tamagnan, G., Kimes, A.S., *et al.* (2000). 5-Iodo-A-85380, an a4b2 subtype-selective ligand for nicotinic acetylcholinereceptors. *Mol. Pharmacol.* **649**, 642–649.

Neve, R.M., Chin, K., Fridlyand, J., Yeh, J., Baehner, F.L., Fevr, T., *et al.* (2006). A collection of breast cancer cell lines for the study of functionally distinct cancer subtypes. *Cancer Cell* **10**, 515–27.

Orimo, A., Gupta, P.B., Sgroi, D.C., Arenzana-Seisdedos, F., Delaunay, T., Naeem, R., *et al.* (2005). Stromal fibroblasts present in invasive human breast carcinomas promote tumor growth and angiogenesis through elevated SDF-1/CXCL12 secretion. *Cell* **121**, 335–48.

Otsuki, Y., Li, Z. & Shibata, M. (2003). Apoptotic detection methods - from morphology to gene. *Prog. Histochem. Cytochem.* **38**, 275–340.

Partridge, A.H., Gelber, S., Peppercorn, J., Ginsburg, E., Sampson, E., Rosenberg, R., *et al.* (2008). Fertility and menopausal outcomes in young breast cancer survivors. *Clin. Breast Cancer* **8**, 65–9.

Pastrana, E., Silva-Vargas, V. & Doetsch, F. (2011). Eyes wide open: a critical review of sphere-formation as an assay for stem cells. *Cell Stem Cell* **8**, 486–98.

Pechoux, C., Gudjonsson, T., Rønnov-jessen, L., Bissell, M.J. & Petersen, O.W. (1999). Human mammary luminal epithelial cells contain progenitors to myoepithelial cells. *Dev. Biol.* **206**, 88–99.

Perou, C.M., Sørlie, T., Eisen, M.B., van de Rijn, M., Jeffrey, S.S., Rees, C., *et al.* (2000). Molecular portraits of human breast tumours. *Nature* **406**, 747–52.

Player, L., Mackenzie, L., Willis, K. & Loh, S.Y. (2014). Women's experiences of cognitive changes or "chemobrain" following treatment for breast cancer: A role for occupational therapy? *Aust. Occup. Ther. J.* **61**, 230–40.

Polyak, K. (2007). Science in medicine Breast cancer : origins and evolution. *J. Clin. Invest.* **117**, 3155–3163.

Ponti, D., Costa, A., Zaffaroni, N., Pratesi, G., Petrangolini, G., Coradini, D., *et al.* (2005). Isolation and In vitro Propagation of Tumorigenic Breast Cancer Cells with Stem / Progenitor Cell Properties Cells with Stem / Progenitor Cell Properties. *Am. Assoc. Cancer Res.* **65**, 5506–5511.

Prevarskaya, N., Skryma, R. & Shuba, Y. (2010). Ion channels and the hallmarks of cancer. *Trends Mol. Med.* **16**, 107–21.

Quintana, E., Shackleton, M., Sabel, M.S., Fullen, D.R., Johnson, T.M. & Morrison, S.J. (2008). Efficient tumour formation by single human melanoma cells. *Nature* **456**, 593–8.

Ricci, A., Greco, S., Mariotta, S., Felici, L., Bronzetti, E., Cavazzana, A., *et al.* (2001). Neurotrophins and neurotrophin receptors in human lung cancer. *Am. J. Respir. Cell Mol. Biol.* **25**, 439–46.

Rosen, P.P., Groshen, S., Saigo, P.E., Kinne, D.W. & Hellman, S. (1989). Pathological prognostic factors in stage I (T1N0M0) and stage II (T1N1M0) breast carcinoma: a study of 644 patients with median follow-up of 18 years. *J. Clin. Oncol.* **7**, 1239–51.

Ruiz-Espejo, F., Cabezas-Herrera, J., Illana, J., Campoy, F.J. & Vidal, C.J. (2002). Cholinesterase activity and acetylcholinesterase glycosylation are altered in human breast cancer. *Breast Cancer Res. Treat.* **72**, 11–22.

Sachlos, E., Risueño, R.M., Laronde, S., Shapovalova, Z., Lee, J.-H., Russell, J., *et al.* (2012). Identification of drugs including a dopamine receptor antagonist that selectively target cancer stem cells. *Cell* **149**, 1284–97.

Sagiv, S.K., Gaudet, M.M., Eng, S.M., Abrahamson, P.E., Shantakumar, S., Teitelbaum, S.L., *et al.* (2007). Active and passive cigarette smoke and breast cancer survival. *Ann. Epidemiol.* **17**, 385–93.

Schaapveld, M., Visser, O., Louwman, M.J., de Vries, E.G.E., Willemse, P.H.B., Otter, R., *et al.* (2008). Risk of new primary nonbreast cancers after breast cancer treatment: a Dutch population-based study. *J. Clin. Oncol.* **26**, 1239–46.

Schuller, H.M. (1989). Cell type specific, receptor-mediated modulation of growth kinetics in human lung cancer cell lines by nicotine and tobacco-related nitrosamines. *Biochem. Pharmacol.* **38**, 3439–42.

Schuller, H.M. (2008). Neurotransmission and cancer: implications for prevention and therapy. *Anticancer. Drugs* **19**, 655–71.

Schuller, H.M. (2009). Is cancer triggered by altered signalling of nicotinic acetylcholine receptors? *Nat. Rev. Cancer* **9**, 195–205.

Seifert, P., Benedic, M. & Effert, P. (2002). Nerve fibers in tumors of the human urinary bladder. *Virchows Arch. an Int. J. Pathol.* **440**, 291–7.

Seifert, P. & Spitznas, M. (2001). Tumours may be innervated. *Virchows Arch.* **438**, 228–231.

Seifert, P. & Spitznas, M. (2002). Axons in human choroidal melanoma suggest the participation of nerves in the control of these tumors. *Am. J. Ophthalmol.* **133**, 711–3.

Sharpe, R., Pearson, A., Herrera-abreu, M.T., Johnson, D., Welti, J.C., Natrajan, R., *et al.* (2012). FGFR signaling promotes the growth of triple negative and basal-like breast cancer cell lines both in vitro and in vivo. *Clin. cancer Res.* **17**, 5275–5286.

Shi, Y., Moon, M., Dawood, S., McManus, B. & Liu, P.P. (2011). Mechanisms and management of doxorubicin cardiotoxicity. *Herz* **36**, 296–305.

Siddiqui, E.J., Shabbir, M., Mikhailidis, D.P., Thompson, C.S. & Mumtaz, F.H. (2006). The role of serotonin (5-hydroxytryptamine1A and 1B) receptors in prostate cancer cell proliferation. *J. Urol.* **176**, 1648–53.

Siegel, R., Naishadham, D. & Jemal, A. (2012). Cancer Statistics , 2012. *A Cancer J. Clin.* **62**, 10–29.

Sleeman, J.P. & Cremers, N. (2007). New concepts in breast cancer metastasis: tumor initiating cells and the microenvironment. *Clin. Exp. Metastasis* **24**, 707–15.

Song, P., Sekhon, H.S., Jia, Y., Carcinoma, C.L., Keller, J.A., Blusztajn, J.K., *et al.* (2003). Acetylcholine is synthesized by and acts as an autocrine growth factor for small cell lung carcinoma acetylcholine is synthesized by and acts as an autocrine growth factor for small cell lung carcinoma. *Cancer Res.* **63**, 214–221.

Song, P. & Spindel, E.R. (2008). Basic and clinical aspects of non-neuronal acetylcholine: Expression of non-neuronal acetylcholine in Lung cancer provides a new target for cancer therapy. *J. Pharmacol. Sci.* **106**, 180–185.

Sourkes, T.L. (2009). Acetylcholine--from Vagusstoff to cerebral neurotransmitter. *J. Hist. Neurosci.* **18**, 47–58.

Spitzmaul, G., Gumilar, F., Dilger, J.P. & Bouzat, C. (2009). The local anaesthetics proadifen and adiphenine inhibit nicotinic receptors by different molecular mechanisms. *Br. J. Pharmacol.* **157**, 804–17.

Starborg, M., Gell, K., Brundell, E. & Höög, C. (1996). The murine Ki-67 cell proliferation antigen accumulates in the nucleolar and heterochromatic regions of interphase cells and at the periphery of the mitotic chromosomes in a process essential for cell cycle progression. *J. Cell Sci.* **109**, 143–53.

Su, G., Zhao, Y., Wei, J., Han, J., Chen, L., Xiao, Z., *et al.* (2013). The effect of forced growth of cells into 3D spheres using low attachment surfaces on the acquisition of stemness properties. *Biomaterials* **34**, 3215–22.

Sumithran, S.P., Crooks, P. a, Xu, R., Zhu, J., Deaciuc, A.G., Wilkins, L.H., *et al.* (2005). Introduction of unsaturation into the N-n-alkyl chain of the nicotinic receptor antagonists, NONI and NDNI: effect on affinity and selectivity. *AAPS J.* **7**, E201–17.

Swain, S.M., Whaley, F.S. & Ewer, M.S. (2003). Congestive heart failure in patients treated with doxorubicin: a retrospective analysis of three trials. *Cancer* **97**, 2869–79.

Takebe, N., Harris, P.J., Warren, R.Q. & Ivy, S.P. (2011). Targeting cancer stem cells by inhibiting Wnt, Notch, and Hedgehog pathways. *Nat. Rev. Clin. Oncol.* **8**, 97–106.

Taly, A., Corringer, P.-J., Guedin, D., Lestage, P. & Changeux, J.-P. (2009). Nicotinic receptors: allosteric transitions and therapeutic targets in the nervous system. *Nat. Rev. Drug Discov.* **8**, 733–50.

Tsang, W.Y. & Chan, K.C. (1992). Neural invasion in intraductal carcinoma of the breast. *Hum. Pathol. Case Stud.* **23**, 202–204.

Urruticoechea, A., Smith, I.E. & Dowsett, M. (2005). Proliferation marker Ki-67 in early breast cancer. *J. Clin. Oncol.* **23**, 7212–20.

Vargo-Gogola, T. & Rosen, J.M. (2007). Modelling breast cancer: one size does not fit all. *Nat. Rev. Cancer* **7**, 659–72.

Ventura, S., Pennefather, J. & Mitchelson, F. (2002). Cholinergic innervation and function in the prostate gland. *Pharmacol. Ther.* **94**, 93–112.

Verbitsky, M., Rothlin, C. V, Katz, E. & Elgoyhen, a B. (2000). Mixed nicotinic-muscarinic properties of the alpha9 nicotinic cholinergic receptor. *Neuropharmacology* **39**, 2515–24.

Veronesi, U., Cascinelli, N., Mariani, L., Greco, M., Saccozzi, R., Luini, A., *et al.* (2002). Twenty-year follow-up of a randomized study comparing breast-conserving surgery with radical mastectomy for early breast cancer. *N. Engl. J. Med.* **347**, 1227–32.

Visvader, J.E. & Lindeman, G.J. (2012). Cancer stem cells: current status and evolving complexities. *Cell Stem Cell* **10**, 717–28.

Weinberg, R. (2014). Coming Full Circle—From Endless Complexity to Simplicity and Back Again. *Cell* **157**, 267–271.

Weiss, S., Dunne, C., Hewson, J., Wohl, C., Wheatley, M., Peterson, a C., *et al.* (1996). Multipotent CNS stem cells are present in the adult mammalian spinal cord and ventricular neuroaxis. *J. Neurosci.* **16**, 7599–609.

De Wever, O. & Mareel, M. (2003). Role of tissue stroma in cancer cell invasion. *J. Pathol.* **200**, 429–47.

Wilkins, L.H., Grinevich, V.P., Ayers, J.T., Crooks, P.A. & Dwoskin, L.P. (2003). N-n-alkylnicotinium analogs, a novel class of nicotinic receptor antagonists: Interaction with a4b2 and a7 neuronal nicotinic receptors. *J. Pharmacol. Exp. Ther.* **304**, 400–410.

Wishart, G.C., Bissett, D., Paul, J., Jodrell, D., Harnett, a, Habeshaw, T., *et al.* (1994). Quinidine as a resistance modulator of epirubicin in advanced breast cancer: mature results of a placebo-controlled randomized trial. *J. Clin. Oncol.* **12**, 1771–7.

Wogan, G.N., Hecht, S.S., Felton, J.S., Conney, A.H. & Loeb, L. a. (2004). Environmental and chemical carcinogenesis. *Semin. Cancer Biol.* **14**, 473–86.

Wong, H.P.S., Yu, L., Lam, E.K.Y., Tai, E.K.K., Wu, W.K.K. & Cho, C.H. (2007). Nicotine promotes cell proliferation via alpha7-nicotinic acetylcholine receptor and catecholamine-synthesizing enzymes-mediated pathway in human colon adenocarcinoma HT-29 cells. *Toxicol. Appl. Pharmacol.* **221**, 261–7.

Woodward, W. a, Chen, M.S., Behbod, F., Alfaro, M.P., Buchholz, T. a & Rosen, J.M. (2007). WNT/beta-catenin mediates radiation resistance of mouse mammary progenitor cells. *Proc. Natl. Acad. Sci. U. S. A.* **104**, 618–23.

Wright, M.H., Calcagno, A.M., Salcido, C.D., Carlson, M.D., Ambudkar, S. V & Varticovski, L. (2008). Brca1 breast tumors contain distinct CD44+/CD24- and CD133+ cells with cancer stem cell characteristics. *Breast Cancer Res.* **10**, R10.

Wu, C.-H., Lee, C.-H. & Ho, Y.-S. (2011). Nicotinic acetylcholine receptor-based blockade: applications of molecular targets for cancer therapy. *Clin. Cancer Res.* **17**, 3533–41.

Wu, Q., Kirschmeier, P., Hockenberry, T., Yang, T.-Y., Brassard, D.L., Wang, L., *et al.* (2002). Transcriptional regulation during p21WAF1/CIP1-induced apoptosis in human ovarian cancer cells. *J. Biol. Chem.* **277**, 36329–37.

Yamashita, M., Ogawa, T., Zhang, X., Hanamura, N., Kashikura, Y., Takamura, M., *et al.* (2012). Role of stromal myofibroblasts in invasive breast cancer: stromal expression of alpha-smooth muscle actin correlates with worse clinical outcome. *Breast Cancer* **19**, 170–6.

Yan, L., Donze, J.R. & Liu, L. (2005). Inactivated MGMT by O6-benzylguanine is associated with prolonged G2/M arrest in cancer cells treated with BCNU. *Oncogene* **24**, 2175–83.

Yvon, a M., Wadsworth, P. & Jordan, M. a. (1999). Taxol suppresses dynamics of individual microtubules in living human tumor cells. *Mol. Biol. Cell* **10**, 947–59.

Zaveri, N., Jiang, F., Olsen, C., Polgar, W. & Toll, L. (2011). Novel alpha3beta4 nicotinic acetylcholine receptor-selective ligands. Discovery, structure-activity studies and pharmacological evaluation. *J. Med. Chem.* **53**, 8187–8191.

Zeng, W., Hu, P., Wu, J., Wang, J., Li, J., Lei, L., *et al.* (2013). The oncolytic herpes simplex virus vector G47Δ effectively targets breast cancer stem cells. *Oncol. Rep.* **29**, 1108–14.

Zhu, B., Heeschen, C., Sievers, R.E., Karliner, J.S., Parmley, W.W., Glantz, S. a, *et al.* (2003). Second hand smoke stimulates tumor angiogenesis and growth. *Cancer Cell* **4**, 191–6.

TABLES

Table 1 . IC_{50} values for compounds tested in sphere-forming assays (MCF7 cells).

	Compound	Reported Receptor Target(s)	IC_{50} (μM ± SD)
Sphere-Formation Inhibitor	**Proadifen**	α3β4, α4β2, α4β4, α1β1δγ	**5.02** ± 2.08
	NDNI	α4β2	**3.75** ± 0.06
	MG 624	α7, α4β2, β2 + β4	**5.37** ± 0.89
	Dicyclomine	M1	**5.12** ± 0.52
	AT-1001	α3β4, α4β2 + α7	33.42 ± 0.12
	Adiphenine	α3β4, α4β2, α4β4, α1β1δγ, M1 and M2	49.14
	Lobeline	α4β2	60.03
	SR 16584	α3β4	129.1
	Memantine	α7, α4β2	178.1
No Effect on Sphere-Formation	Dihydro-β-Erythrodine	α4β2, α4β4	>250
	5-iodo-A-85380	α4β2	>250
	Methyllycaconitine	α7, and α3/α6β2β3	>250
	Mecamylamine	α4β2, α4β4, α2β4, α2β2, α7	>250
	α-Bungarotoxin	α7 + α9	>250
	Strychnine	α7, α9 + α4β2	>250
	Atropine	α9, M1-M5	>250
	Scopolamine	M1	>250
	Tubocurarine	α9, α7, α3β4	>250

Table 2. Molecular structures of the top 4 hit AChR inhibitors.

Compound	Structure	Compound	Structure
NDNI	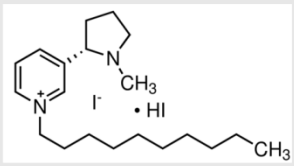	Proadifen	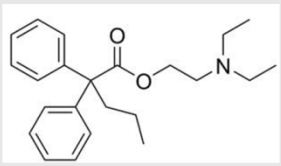
MG 624	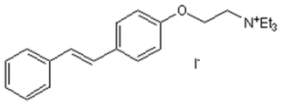	Dicyclomine	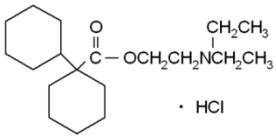

Table 3. MG624 IC_{50} generated from sphere-forming assays in different breast cancer cell lines and X81 PDX cells.

Cell Line	Gene Cluster	ER	PR	HER2	MG624 IC_{50} (µM) ± SD	Approximate MG624 "Residual" Secondary IC_{50} (µM)
HCC1954	Basal	-	-	+	3.52 ± 0.34	0.105 ± 0.03
ZR-751	Luminal	+	-	-	12.74 ± 1.29	2.5 - 5
BT-474	Luminal	+	+	+	11.05 ± 0.87	0.156 – 0.3125
MCF-7	Luminal	+	+	-	5.37 ± 0.89	0.3125 – 0.625
T47D	Luminal	+	+	-	1.87 ± 0.32	0.3125 – 0.625
MDA-MB-453	Luminal	-	-	+	1.26 ± 0.91	N/A
X81 (PDX)	**Luminal B**	**+**	**-**	**-**	**5.09** ± 1.07	**0.156 – 0.3125**

FIGURES

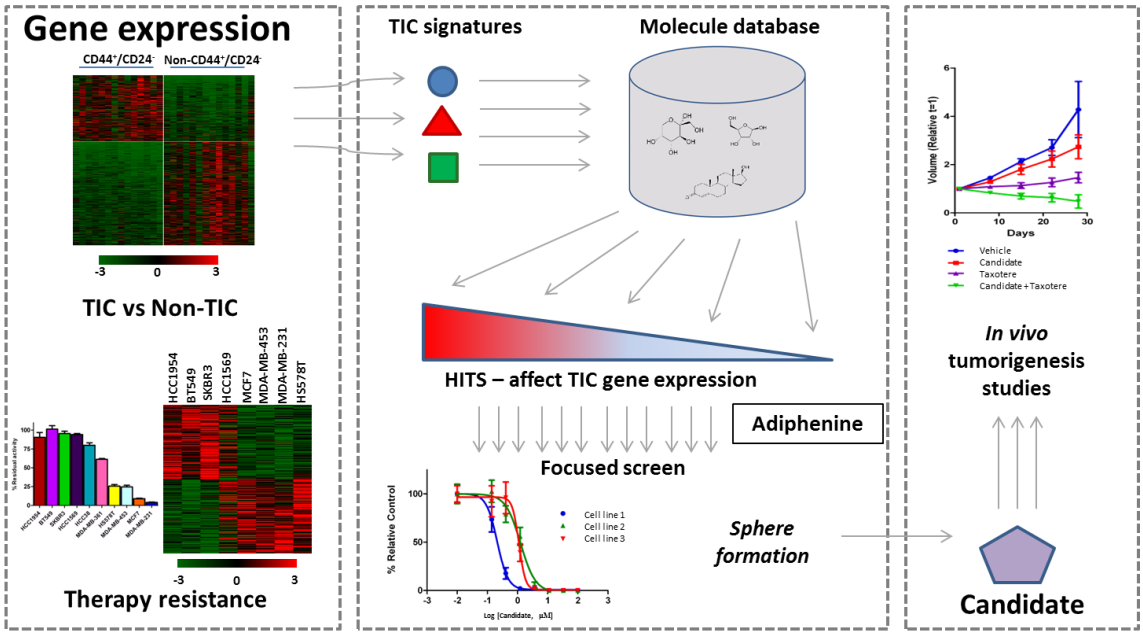

Figure 1. The discovery of nAChR antagonists as potential anti-TIC compounds. Adiphenine (an AChR antagonist) was identified through connectivity mapping using two independent gene signatures: a TIC phenotypic signature using differential gene expression between breast tumor cells expressing $CD44^{+}/CD24^{-/low}$ vs. other, and the differential gene expression between chemoresistant vs. sensitive breast cancer cell lines. Focused screens (including chemosensitization assays and sphere-forming assays) revealed nAChR antagonists specifically inhibit sphere-forming cells and chemosensitize breast cancer cells. Therefore nAChR antagonists became the chemical class of interest. Image provided by Dr. Robin Hallett (Hassell Lab, McMaster University).

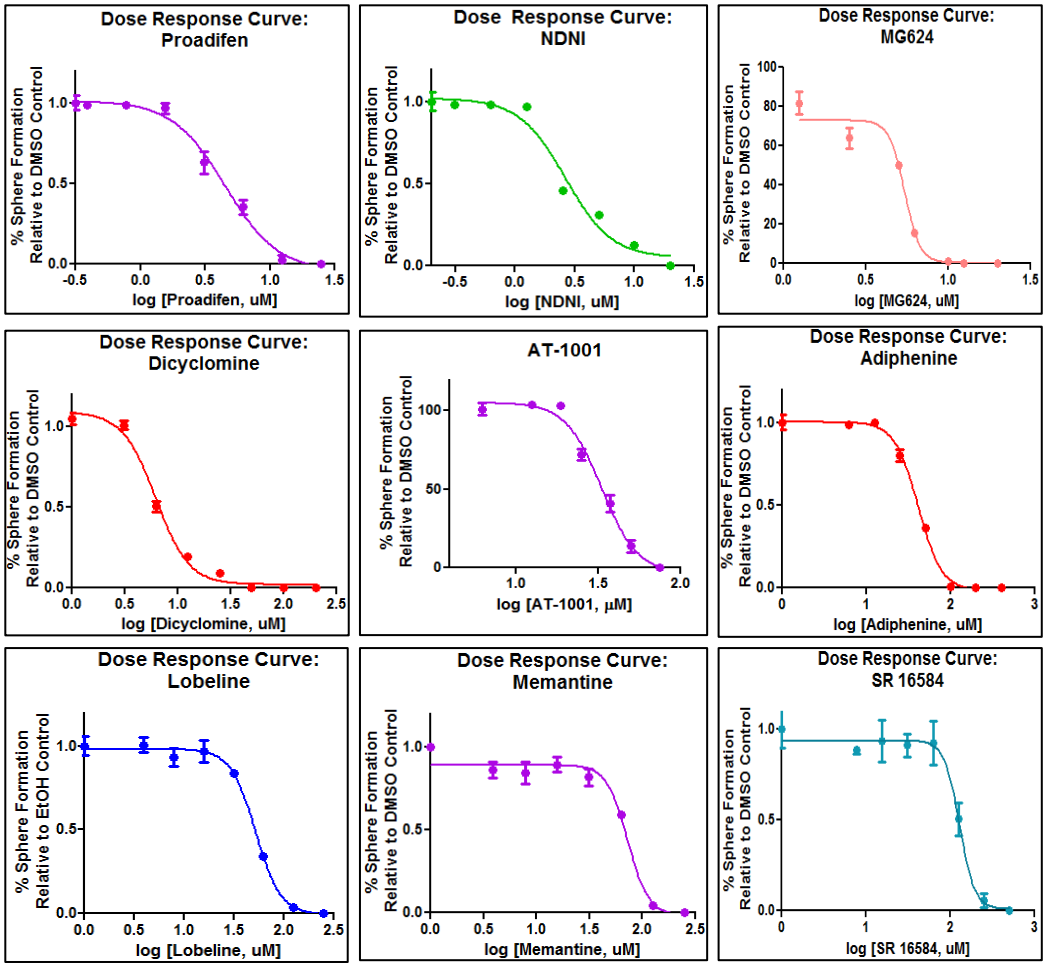

Figure 2. nAChR antagonists inhibit sphere formation in MCF7 cells. Nine out of the 18 AChR antagonists tested successfully inhibited sphere formation in MCF7 cells; 8 nAChR antagonists, and 1 mAChR antagonist (See Table 1). Compounds that failed to inhibit sphere formation by at least 50% of the control at 250µM were considered inactive (Appendix 1).

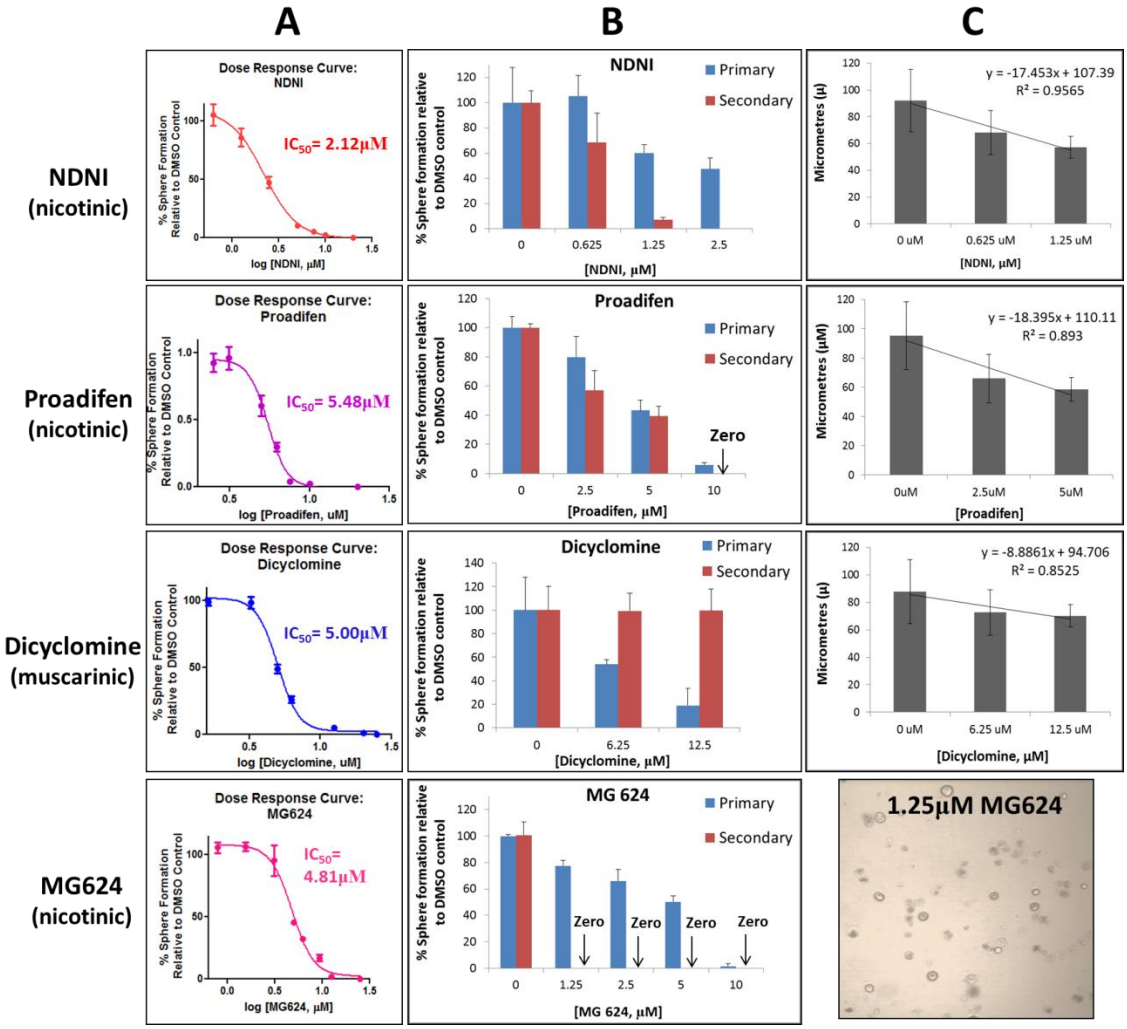

Figure 3. nAChR antagonists irreversibly target human sphere-forming cells. A) Primary sphere-forming assays for the 4 most potent AChR antagonists: NDNI, Proadifen, Dicyclomine and MG624 in HCC1954 spheres. B) Comparison between primary and secondary sphere numbers to test for compound irreversibility. C) Decreasing secondary sphere sizes with increasing treatment doses. All p-values < 0.05. Bottom right image: Secondary single cells from lowest MG624 dose (no secondary spheres formed in MG624-treatment wells). See Appendix 3 for corresponding images from primary and secondary sphere-forming assays for NDNI, proadifen, dicyclomine and MG624.

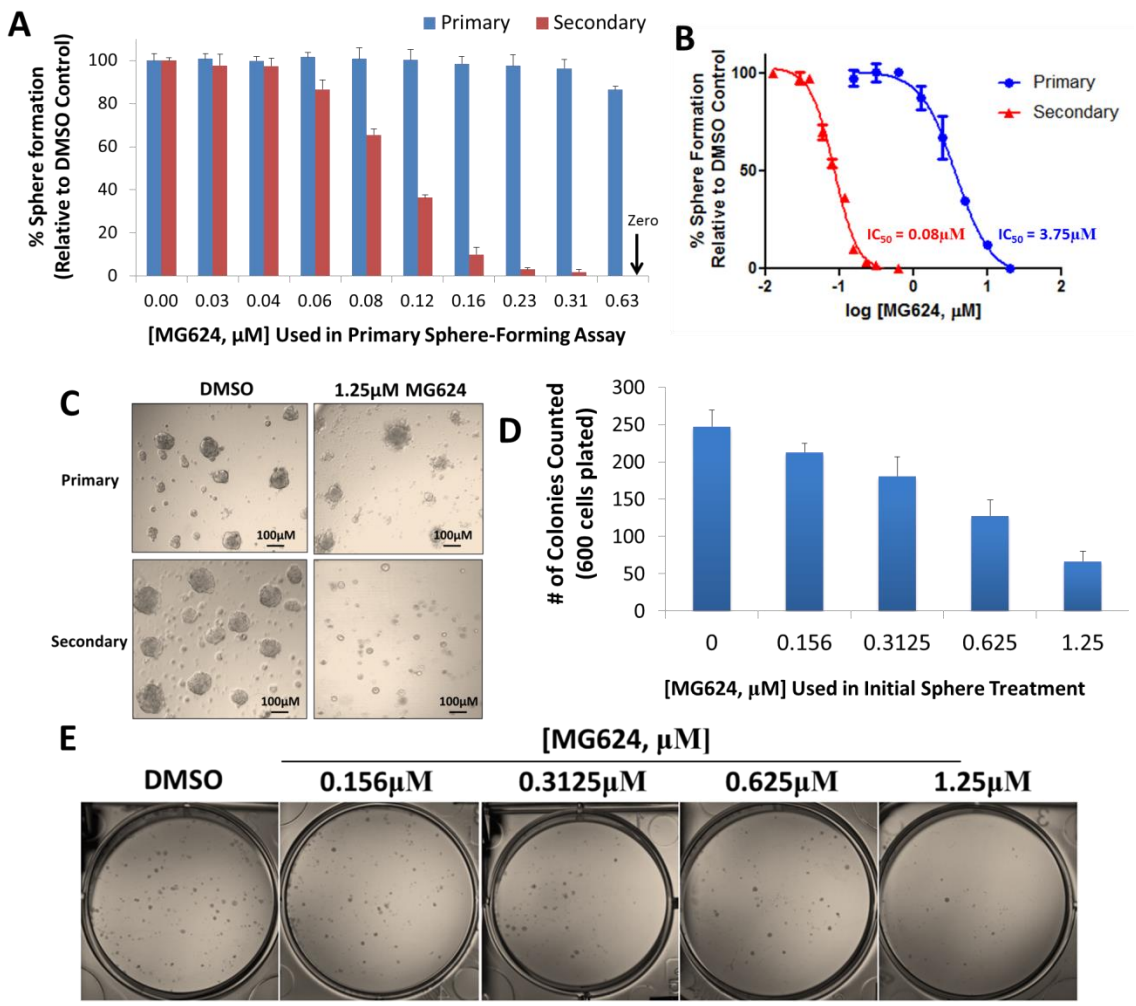

Figure 4. MG624 displays high specificity for sphere-forming cells over other cells *in vitro*. A) Comparison between primary and secondary sphere formation across 10 doses of MG624 in HCC1954 spheres. B) Comparison between primary and secondary IC_{50} values based on the data in panel A. The "secondary IC_{50} curve" represents a residual IC_{50} curve, as this is the effect of MG624 after spheres were exposed to MG624 for 4 days, were dissociated, and were seeded in a new assay (no inhibitors present). C) Primary versus secondary HCC1954 spheres treated with either DMSO or 1.25µM MG624. D&E) Spheres that were treated with MG624 for 4 days were dissociated and seeded into a colony-forming assay, in serum-containing media, a read out of the proliferative capabilities of all cells remaining in culture. Plates were incubated for 10 days. D) Colony numbers counted following incubation. Error bars represent the standard deviation observed between 3 replicates. E) Representative images of the colonies quantified in (D).

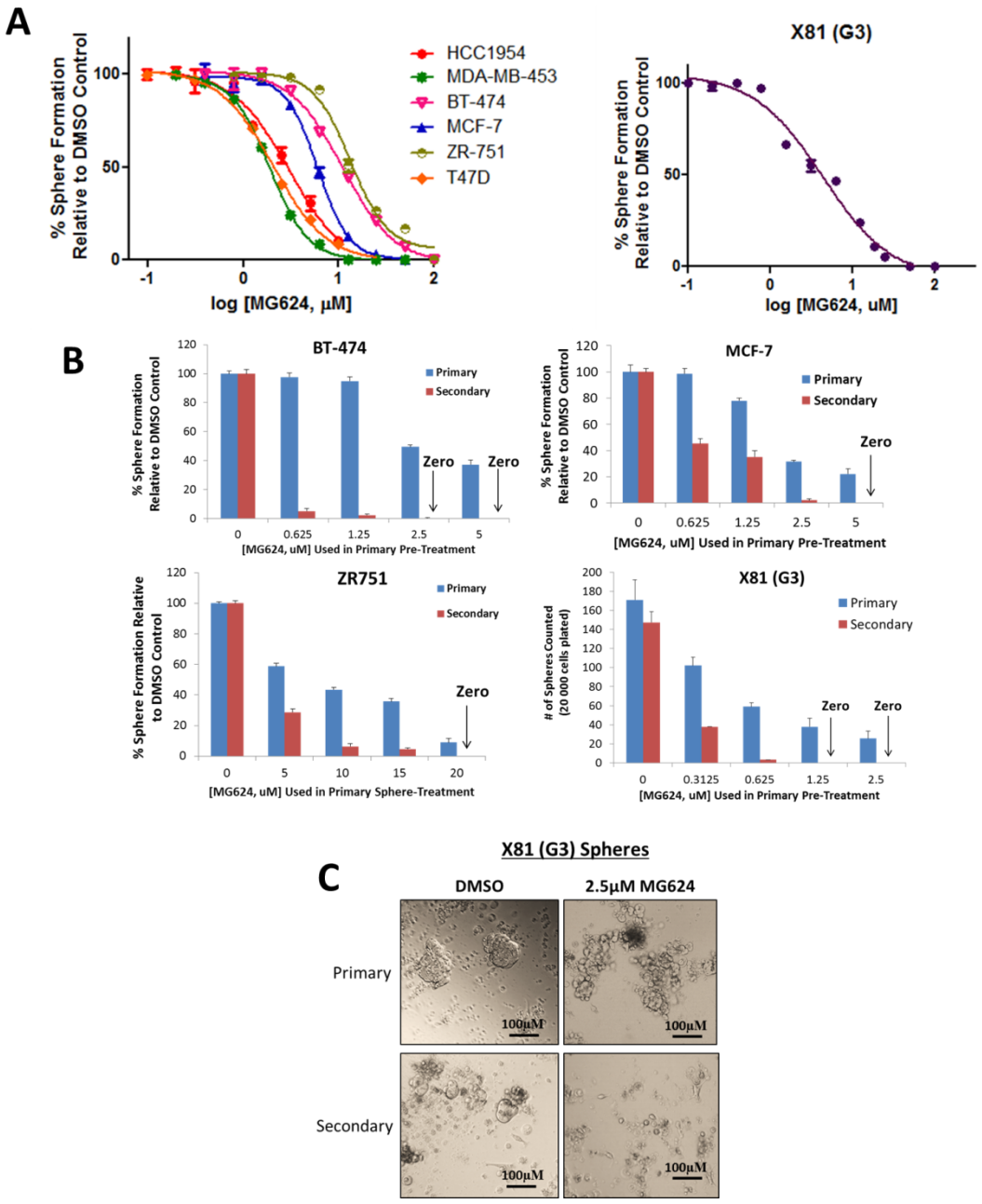

Figure 5. MG624 specifically inhibits sphere-forming cells in 6 cell lines and X81 PDX spheres. A) Left image: Sphere-forming assays across 6 different breast cancer cell lines. Right image: Sphere-forming assay in patient-derived xenograft X81. B) Primary vs. secondary sphere-forming assays in BT-474, MCF-7 and ZR751 cell lines, and in PDX X81 cells, propagated as spheres. C) Images of X81 spheres in primary and secondary sphere-forming assays.

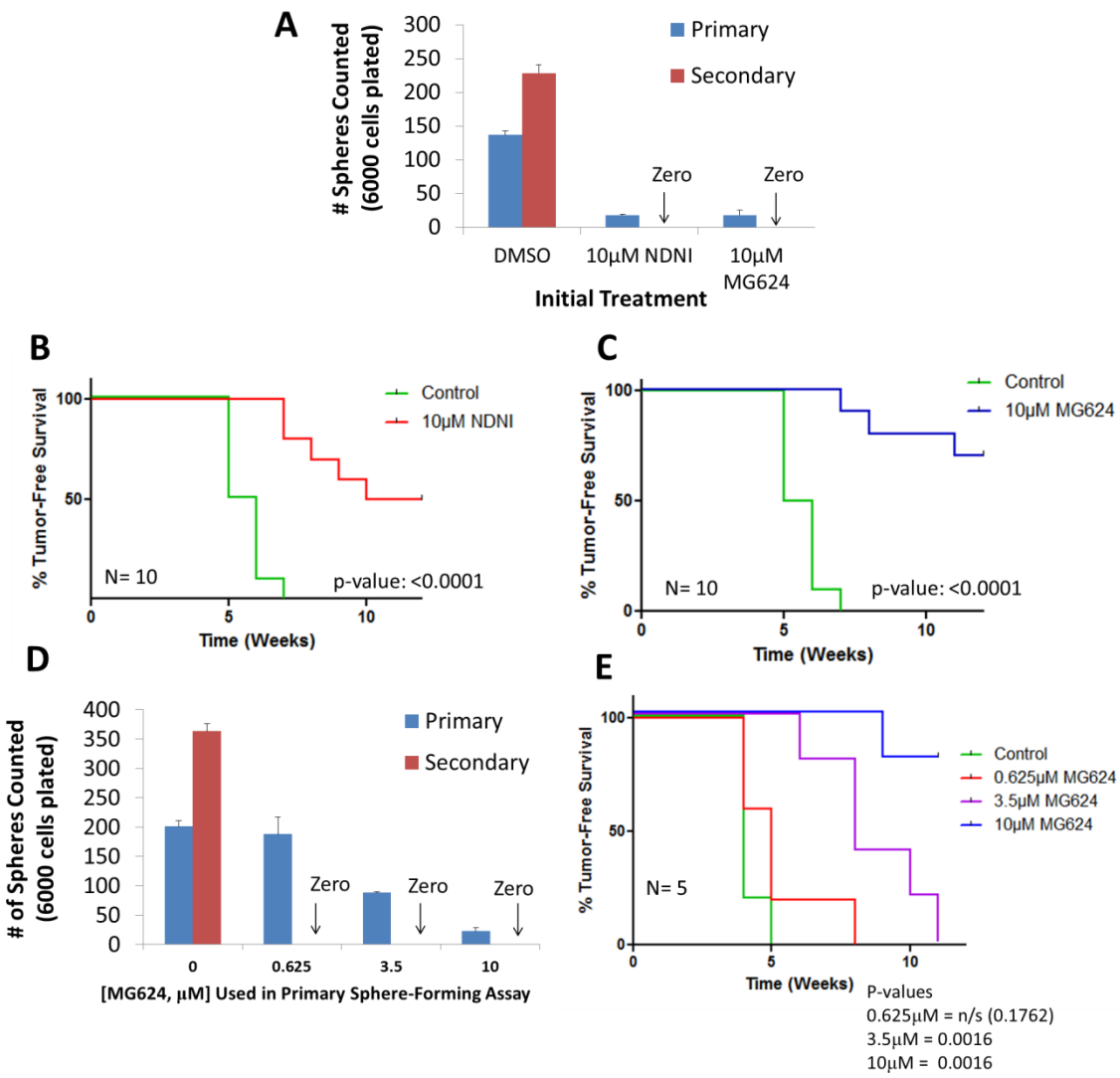

Figure 6. nAChR antagonists target functional breast tumor-initiating cells.
A) Cells that were treated with 10µM of either NDNI or MG624 were seeded in a secondary sphere-forming assay as a control. B&C) *Ex vivo* transplantation of 17 500 viable HCC1954 cells (derived from spheres) treated with either B) NDNI or C) MG624 or the vehicle (control). D) Cells were treated with increasing concentrations of MG624 before being seeded into a secondary sphere-forming assay as a control. E) *Ex vivo* transplantation of 60 000 viable HCC1954 cells (derived from spheres) treated with increasing doses of MG624 or the vehicle.

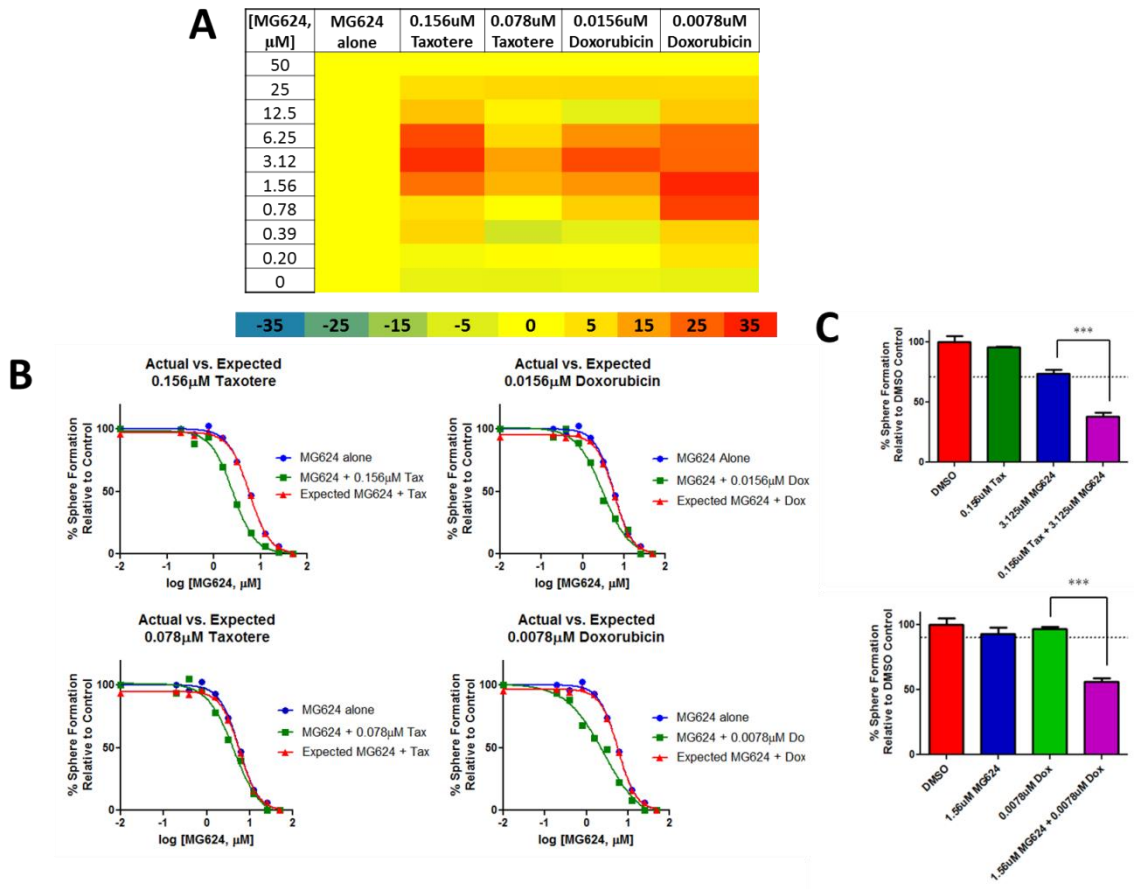

Figure 7. MG624 synergizes with chemotherapy to inhibit sphere-formation *in vitro*. Increasing doses of MG624 were combined with either 0.156 or 0.078µM taxotere or 0.0156 or 0.0078µM doxorubicin to generate IC_{50} curves. A) Heat map of the effect of MG624 and chemotherapy on sphere inhibition. Red indicates doses found to inhibit spheres greater than an additive effect of both treatments. B) Expected MG624 and taxotere IC_{50} curves (red) were compared to the actual IC_{50} curves observed through sphere quantifications normalized to the control (taxotere or doxorubicin alone, green) and the IC_{50} curve of MG624 alone (blue). C) Bar graphs demonstrating the doses of MG624 and taxotere or MG624 and doxorubicin that showed the greatest synergy. The dotted line indicates the expected effect of MG624 and taxotere or MG624 and doxorubicin, if treatments were additive. All p-values <0.001.

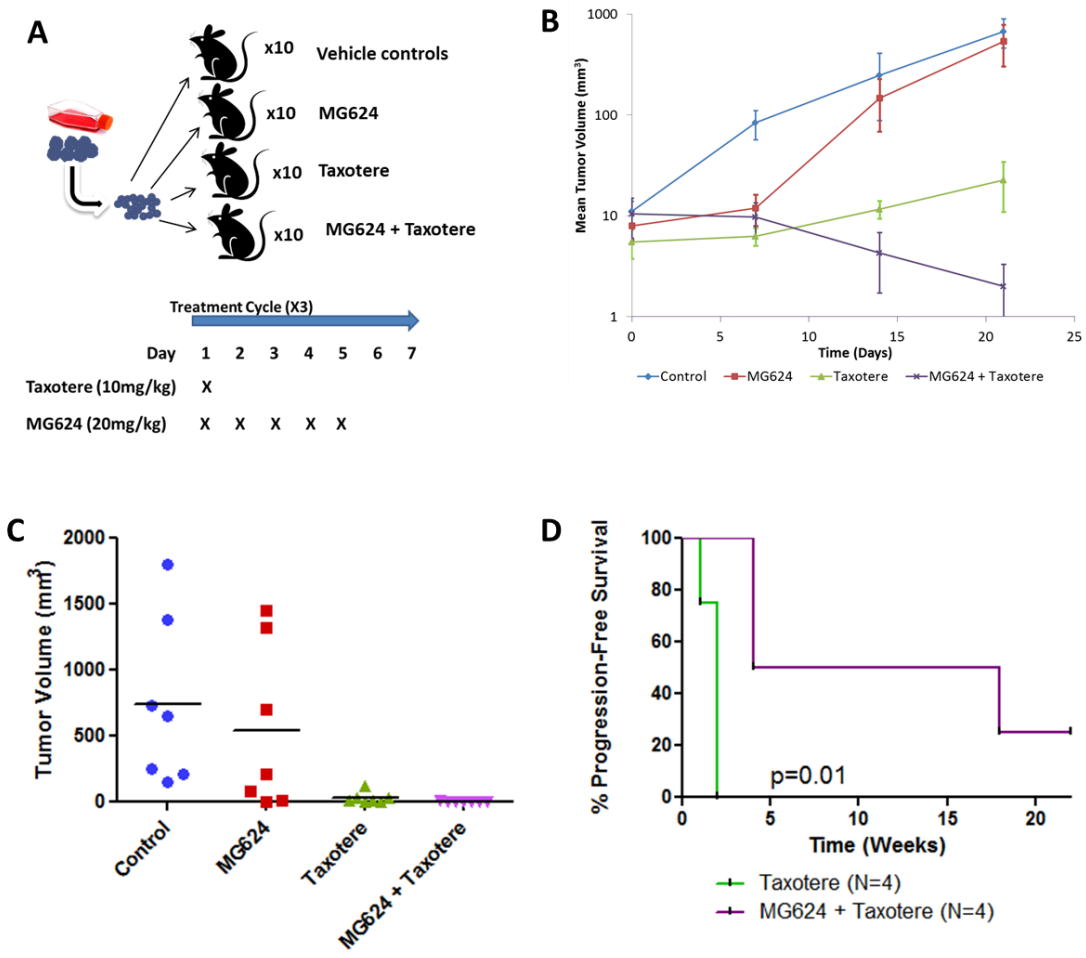

Figure 8. MG624 combined with chemotherapy significantly inhibits tumor growth and prevents tumor progression post-treatment. HCC1954-tumor bearing NOD/SCID mice were treated with vehicle (control), MG624, taxotere, or MG624 + taxotere. A) Experiment set up and dosing regimen. B) Mean tumor volumes in mice treated with vehicles (control), MG624 (20mg/kg), Taxotere (10mg/kg), or both MG624 and Taxotere over the course of the three week treatment regimen. C) Mean tumor volumes at the end of treatment (day 21). D) Tumor progression/recurrence follow-up.

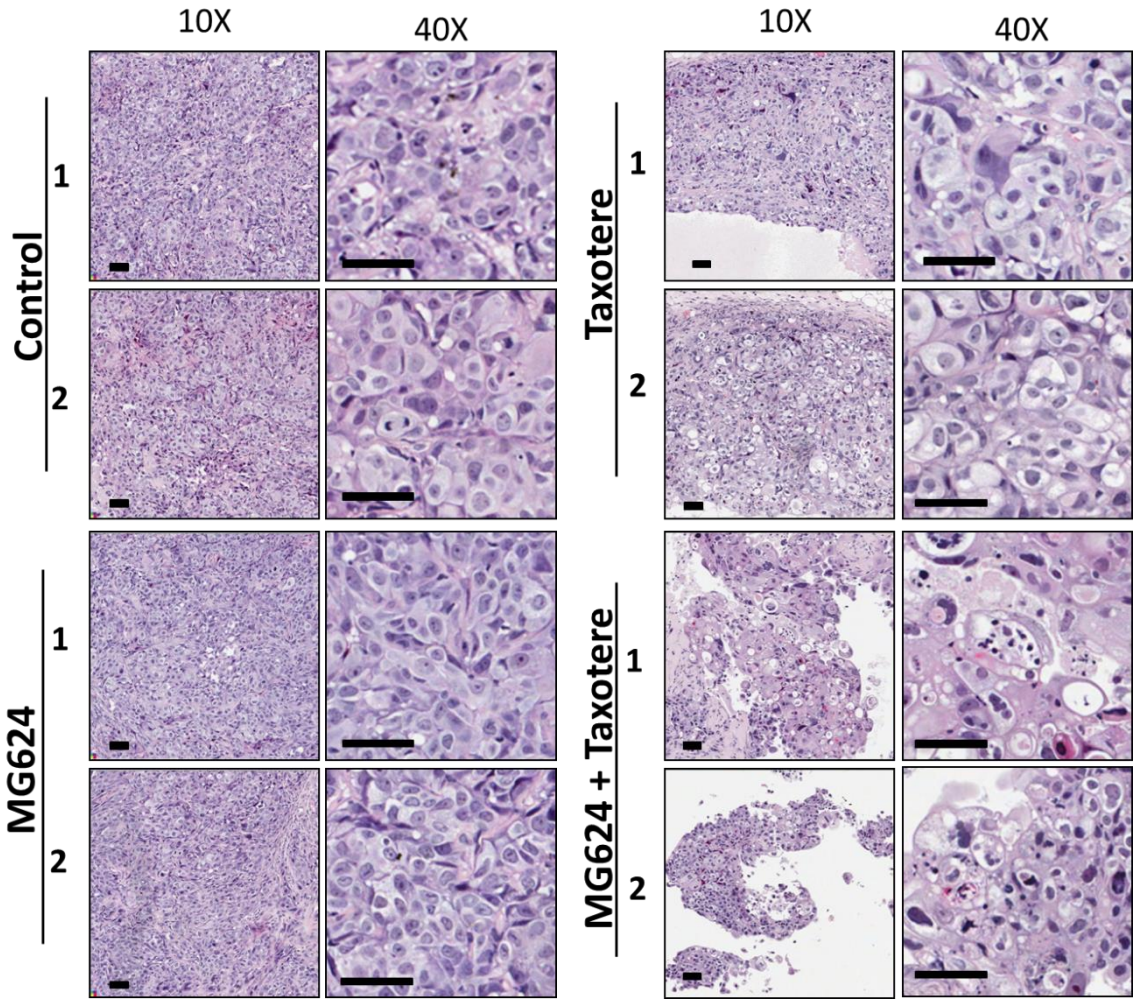

Figure 9. Tumors treated with a combination of MG624 and Taxotere display unique cell morphology. H & E of 2 tumors per cohort post-treatment with vehicle, MG624, taxotere, or MG624 and taxotere combined. Scale bar = 100μm.

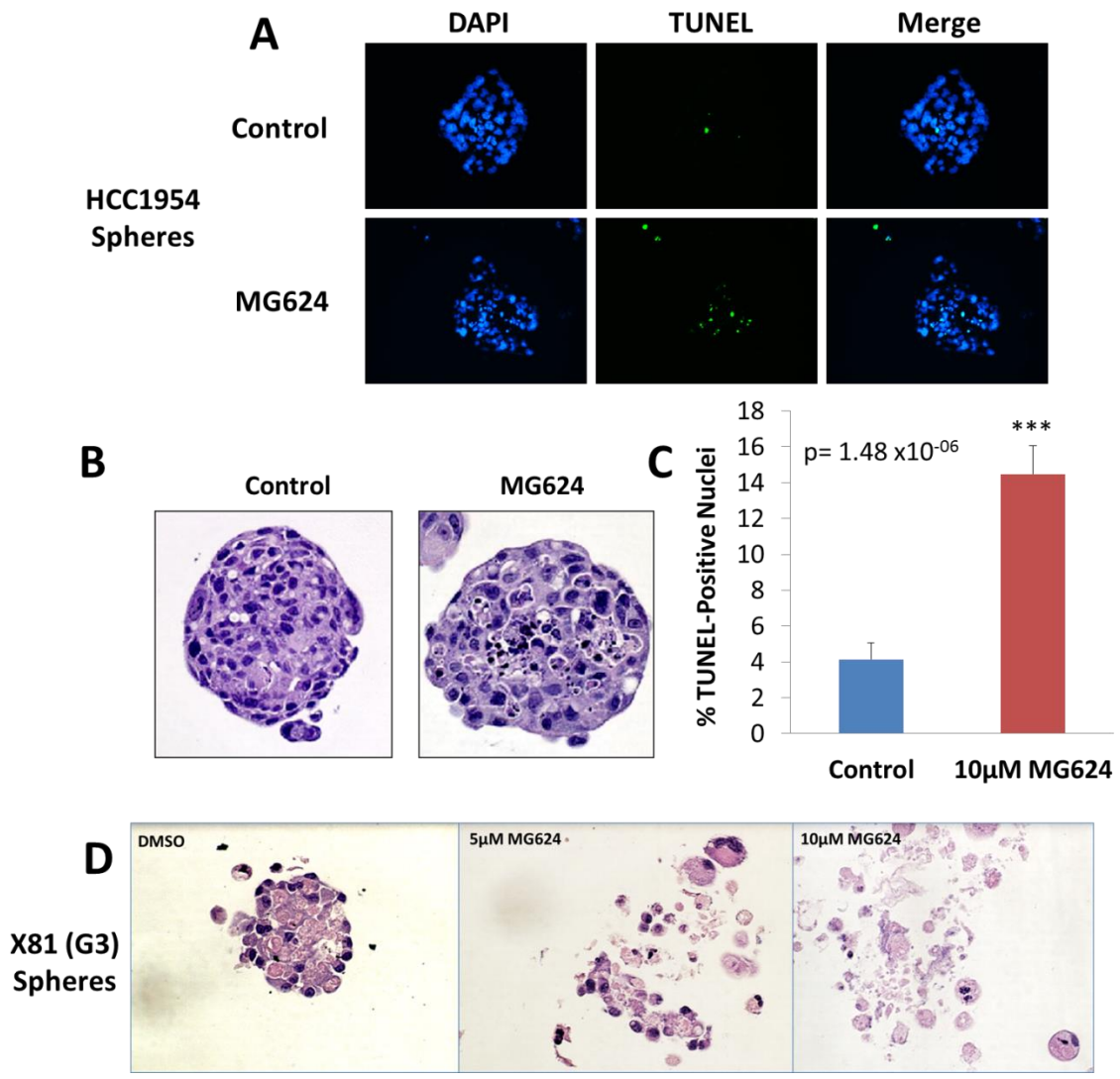

Figure 10. MG624 induces apoptosis in established spheres after 48 hours of treatment. A) HCC1954 spheres were grown for 4 days before 10µM of MG624 was added to the media (or DMSO control). After 48 hours of exposure, spheres were fixed and embedded, and sections of the sphere block were stained with TUNEL to detect fragmented DNA. B) H&E stain of HCC1954 sphere block sections after 48 hours of treatment with either DMSO or 10µM MG624. C) Quantification of percent TUNEL positive nuclei in five HCC1954 spheres treated with 10µM MG624 compared to five spheres treated with DMSO for 48 hours. D) H&E stain of PDX X81 xenograft cells grown as spheres for 7 days, and treated with either DMSO, 5 or 10µM of MG624 for 48 hours before being fixed, embedded and sectioned.

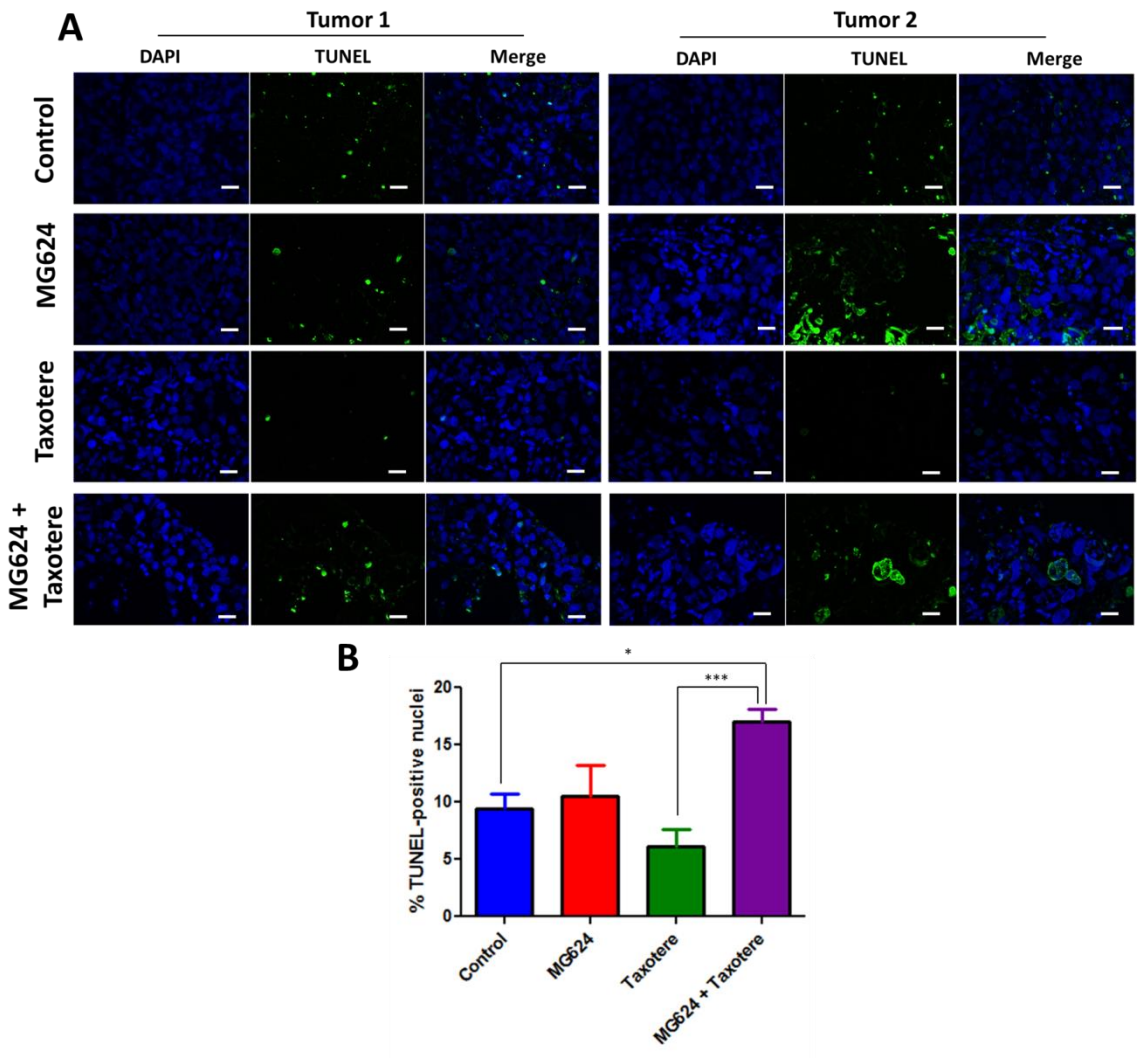

Figure 11. MG624 combined with chemotherapy induces apoptosis in tumor cells. HCC1954-tumor bearing NOD/SCID mice were treated with vehicle, MG624, taxotere, or MG624 + taxotere for 3 weeks. Fragmented nuclei (characteristic of apoptotic cells) were detected via TUNEL assay. A) TUNEL staining of two tumors per treatment cohort. Scale bar = 50µM. B) Total nuclei and TUNEL-positive nuclei were counted in four fields of view at 40X magnification to generate a mean % TUNEL-positive nuclei ± SEM for each tumor (2 tumors per treatment). $p = 0.0015$.

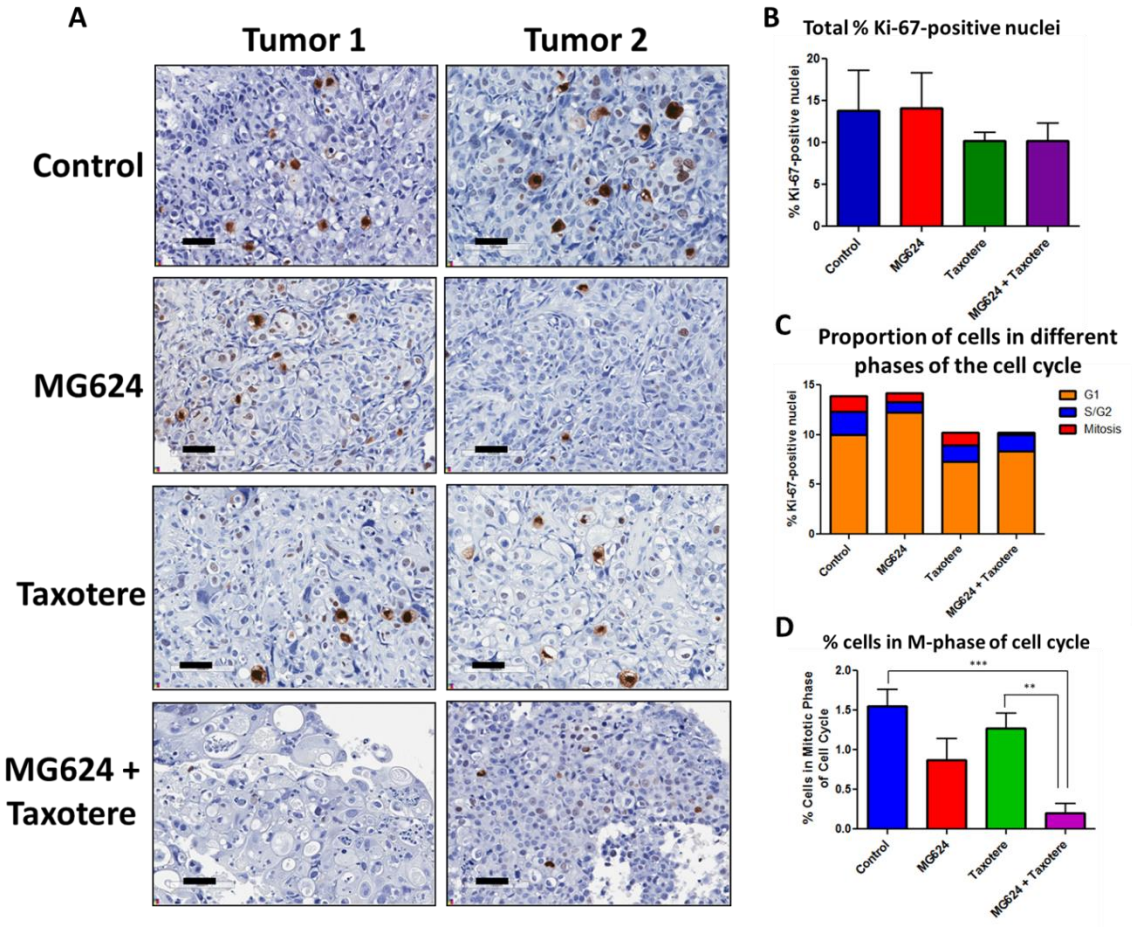

Figure 12. MG624 combined with chemotherapy reduces tumor cell mitosis. HCC1954-tumor bearing NOD/SCID mice were treated with vehicle, MG624, taxotere, or MG624 + taxotere for 3 weeks. Tumor sections were stained for the Ki-67 protein, a marker of cell proliferation. A) IHC for Ki-67, two tumors per treatment cohort. Scale bar = 50µm. B) Total nuclei and Ki-67-positive nuclei were counted in 3 fields of view at 20X magnification to generate a mean % Ki-67-positive nuclei ± SEM for each tumor (2 tumors per treatment). Differences were not significant. C) The proportions of Ki-67-positive nuclei in different phases of the cell cycle, based on staining localization/intensity. D) Mean % cells in M-phase of cell cycle (based on staining intensity and cell size/morphology). p = 0.0009.

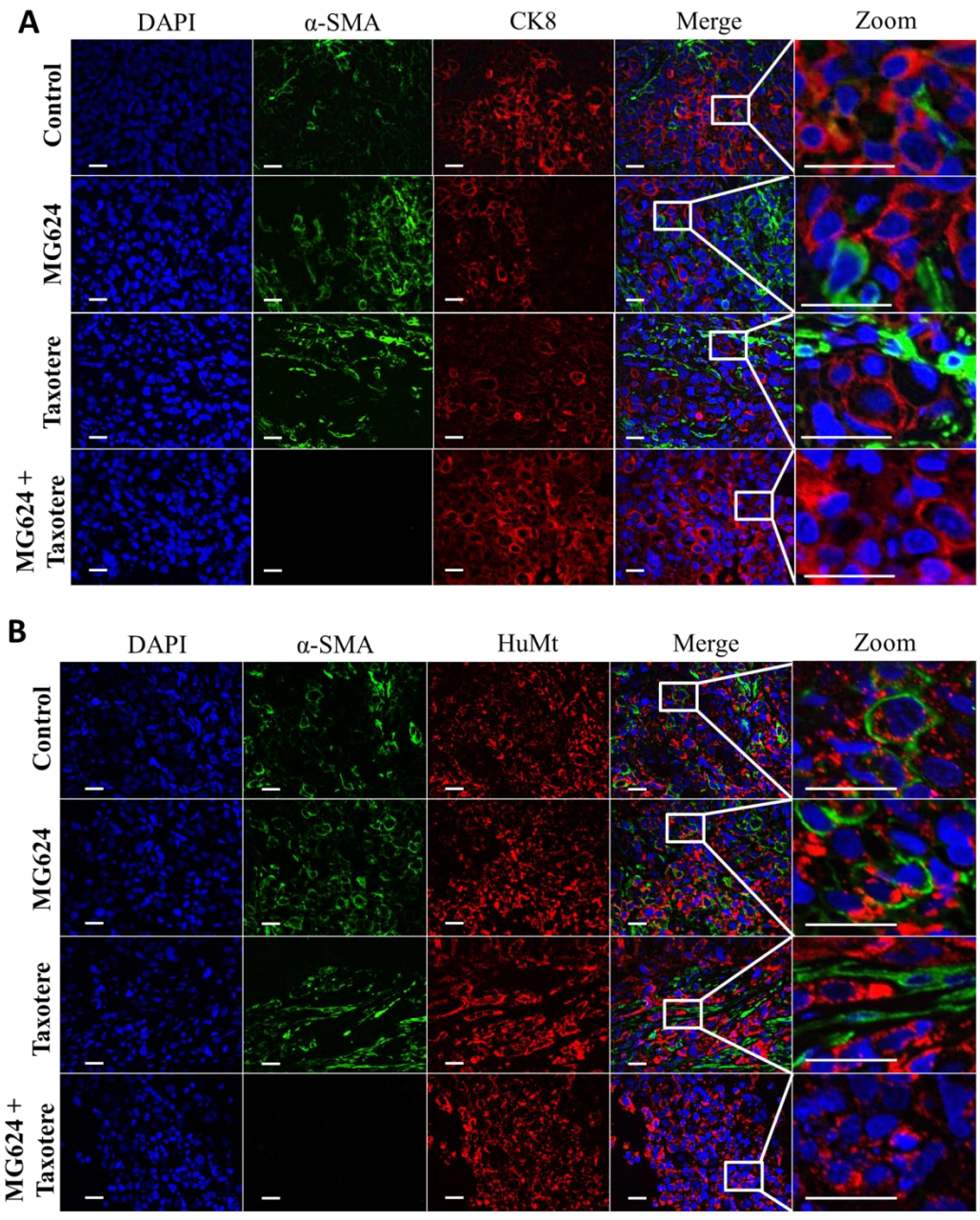

Figure 13. MG624 combined with chemotherapy eliminates intratumoral fibroblasts and stromal cells, and enriches for CK8$^+$ cells. Tumor sections from mice treated with vehicle, MG624, taxotere, or MG624 + taxotere for 3 weeks. Tumor sections were stained for α-SMA and CK8 to check for tumor cell lineage differences between treatments. A) α-SMA andCK8 staining for all 4 cohorts, where the combination of MG624 and taxotere enriched for CK8$^+$ cells. B) HuMt (and α-SMA) staining to differentiate human α-SMA-positive tumor cells and stromal cells. α-SMA-positive cells in taxotere sections are not human, and are thus most likely mouse fibroblasts. Scale bars = 50μM.

APPENDIX

1. *Sphere-forming assay IC_{50} curves for inactive compounds in MCF7 cells*

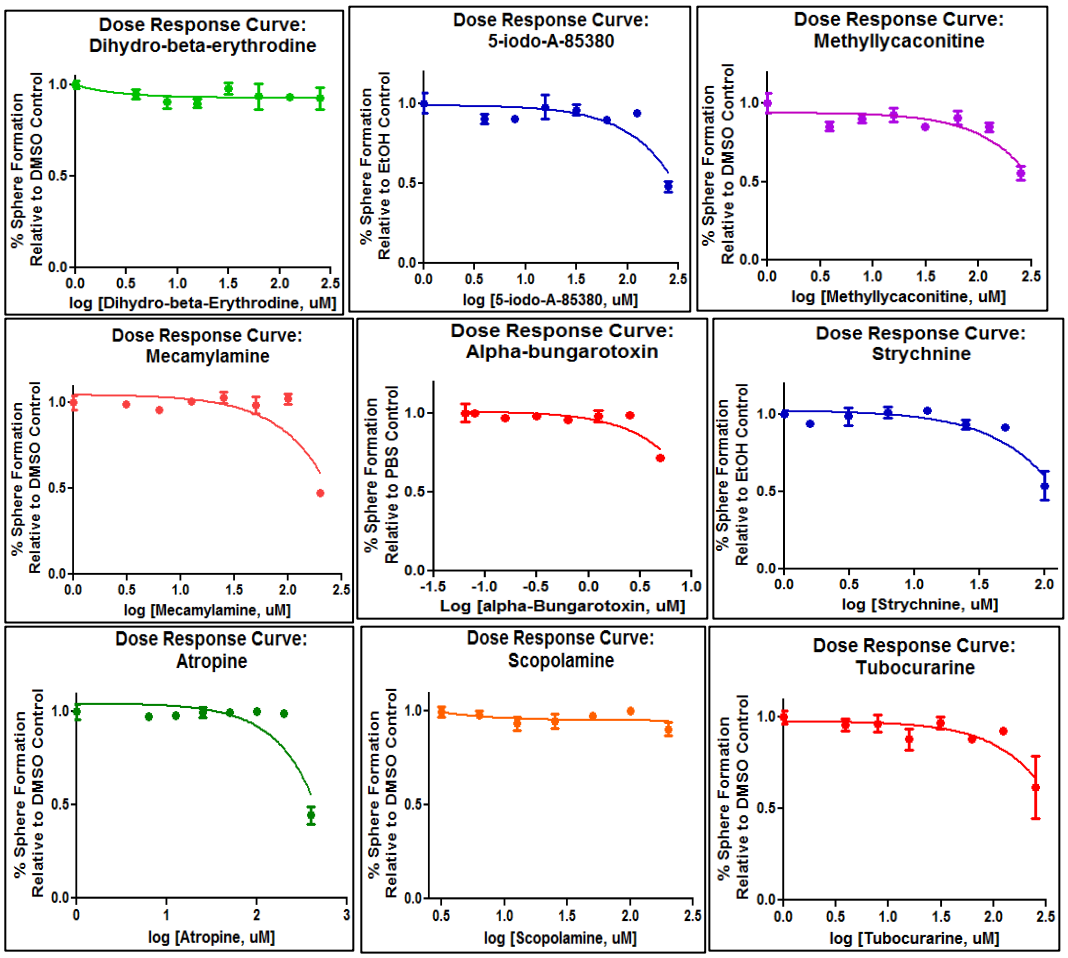

Appendix Figure 1. Not all nAChR antagonists inhibit sphere formation in MCF7 cells. Nine out of 18 AChR antagonists tested did not inhibit sphere formation in MCF7 cells; 7 nAChR antagonists and 2 mAChR antagonists (see Table 1).

2. *PrestoBlue® cell viability assays*

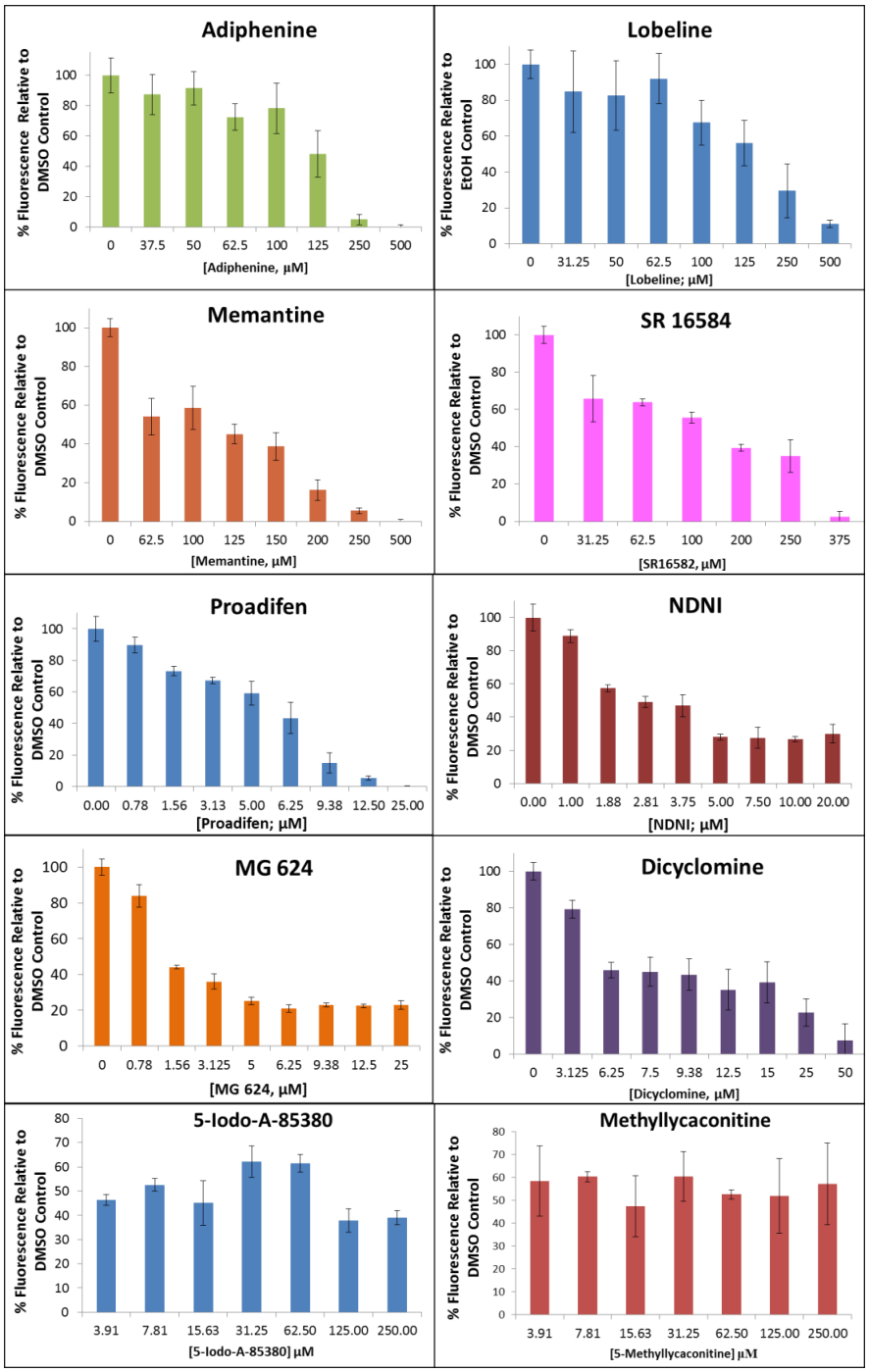

Appendix Figure 2. PrestoBlue® assays validate sphere-forming assay findings.

3. Primary and secondary sphere-forming assay images (see Figure 2).

NDNI

Primary

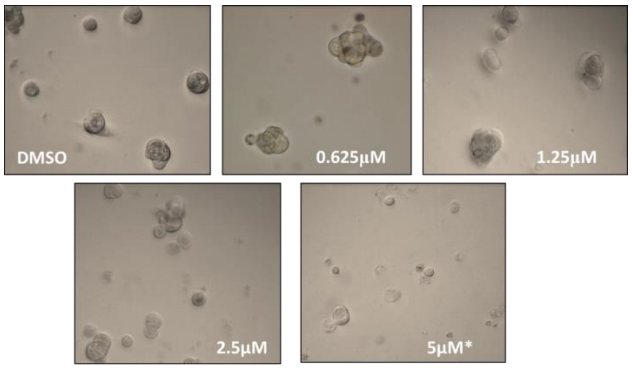

Secondary

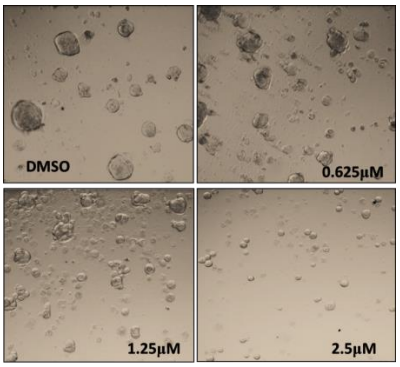

Proadifen

Primary

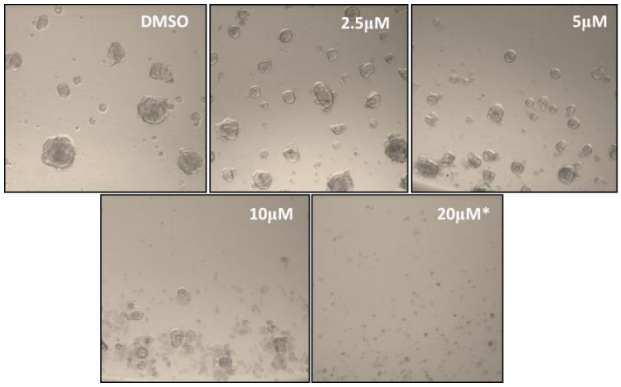

Secondary

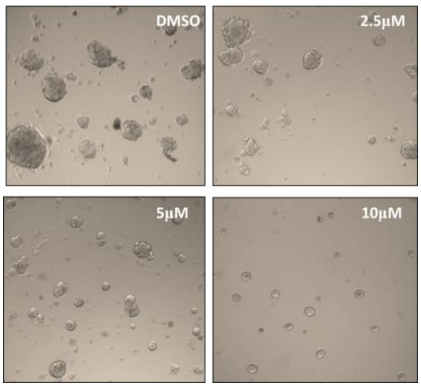

Dicyclomine

Primary

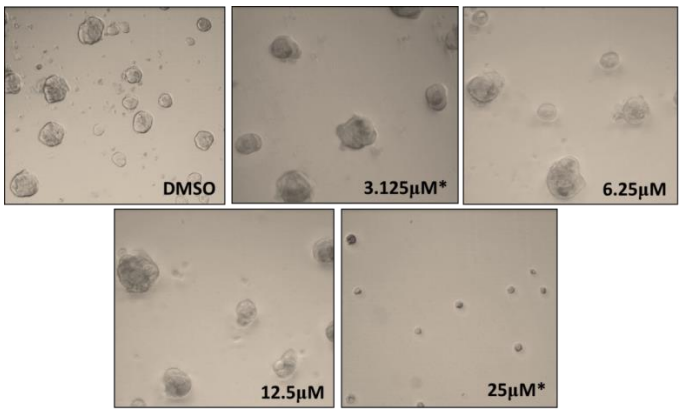

Secondary

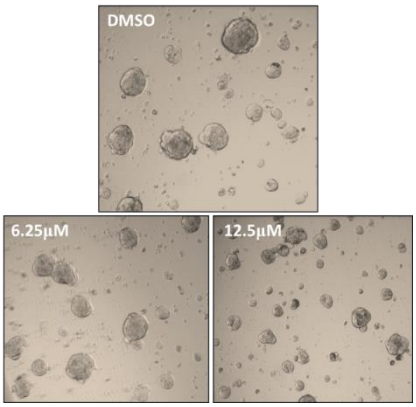

MG624

Primary

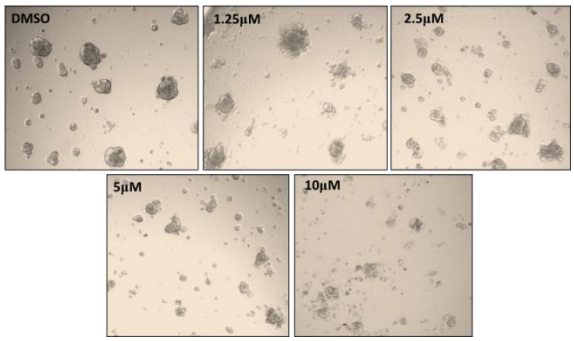

Secondary

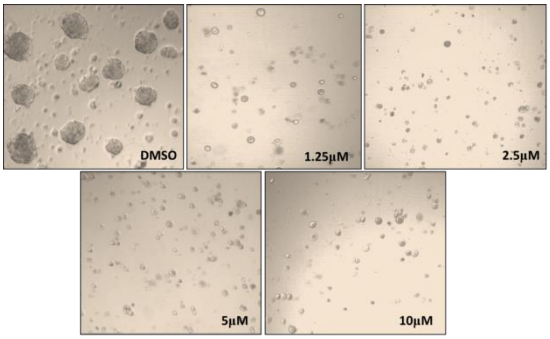

Appendix Figure 3. Primary and secondary sphere forming assay images from the four most potent compounds in HCC1954 cells.

4. Colony forming assays in the presence of MG624

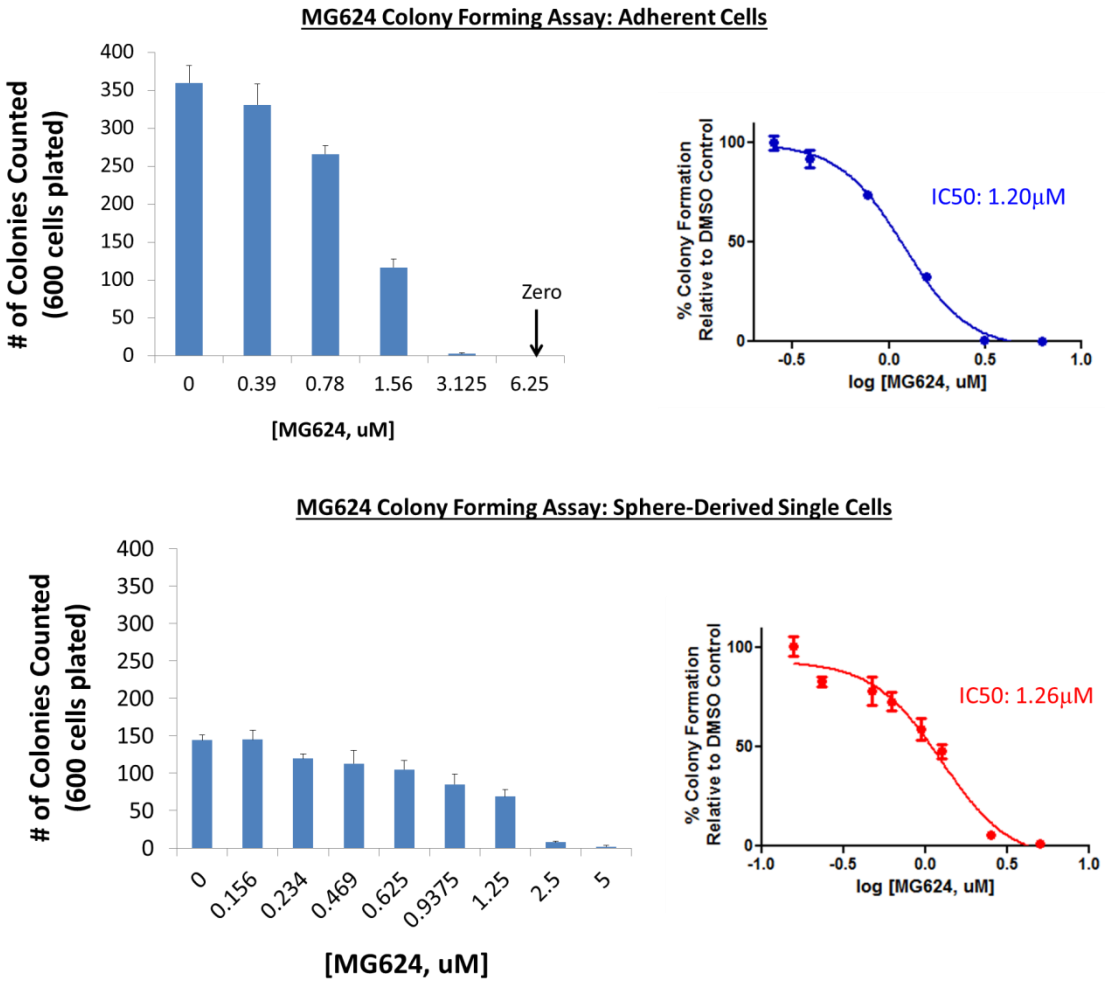

Appendix Figure 4. Colony forming assays performed in the presence of MG624. HCC1954 single dispersed cells derived from either an adherent culture (top figures) or from dissociated spheres (bottom images) were seeded at 600 cells per well in a 6-well plate. Increasing concentrations of MG624 were then added to the wells in triplicate. Plates were incubated for 10 days.